THE UNIVERSITY OF MICHIGAN
RADIO ASTRONOMY OBSERVATORY

OGO-III DATA ANALYSIS:
DYNAMIC SPECTRA OF SOLAR BURSTS

Thomas E. Graedel

NASA Grant NGR-23-005-~~311~~ 312
Final Scientific Report

DEPARTMENT OF ASTRONOMY

Preface

This paper constitutes the final scientific report for NASA Grant NGR-23-005-311, "OGO-III Data Analysis: Dynamic Spectra of Solar Bursts." The work described herein was performed by the author, in consultation with personnel at the University of Michigan Radio Astronomy Observatory.

The impetus for this research was the promising results obtained during the initial analysis of the data from the University of Michigan experiment aboard OGO-III (Graedel, 1969). In that analysis, the trial approach of using a simplified model to construct time profiles of solar radio bursts proved able to restrict the ranges of certain parameters of the overall emission mechanism. It was felt that an extension of this approach over a wide frequency range would delineate some of the parameters still more accurately. Such has proven to be the case, although in many ways the results pose more questions than they answer.

The author acknowledges with thanks the assistance of W. H. Potter and S. L. Breckenridge in supplying computer programs and advice, and of W. H. Schoendorf for helpful scientific discussions.

Table of Contents

I. History of the Problem

A. Introduction

The most frequent of the many forms of solar radio emission is the Type III (fast-drift) burst. Type III bursts occur at frequencies as high as 550 MHz (Malville, 1967) and at least as low as 100 KHz (Haddock and Graedel, 1968). Their characteristics at the higher frequencies have been well determined (see, for example, Kundu, 1965), and recent space experiments (Graedel, 1969; Hartz, 1969; Stone, 1969) have extended the study to frequencies below the atmospheric cutoff.

The general features of the theoretical development of Type III bursts have been established for some time (cf. Wild, Smerd, and Weiss, 1963). As the number and frequency range of observations has increased, however, the need for model refinement has become increasingly apparent (Newkirk, 1967; Slysh, 1967; Hartz, 1969). The work described herein was undertaken with the expectation of providing new information on the burst processes, and with the hope of establishing more stringent guidelines for a comprehensive theoretical attack on the problem of Type III solar radio emission.

B. Mechanisms for Type III Bursts

The present theory of Type III bursts is as follows: a stream of electrons, with velocities of several tenths of the speed of light, is injected into the corona at or near its base. It then propagates radially outward, setting up electron plasma waves at each point along its path. These electron plasma waves, which oscillate in a small band of frequencies centered on the local plasma frequency, are converted to electromagnetic waves by scattering off small-scale fluctuations of the plasma density. Collisions between electrons and ions then act to damp out the plasma oscillations, and hence the electromagnetic radiation.

Early observations of solar radio bursts (Payne-Scott, Yabsley, and Bolton, 1947) suggested that the enhancement of radiation from a burst occurred successively later in time at lower frequencies. Since the coronal electron density decreases outward from the sun, this observation suggested a moving disturbance which resulted in radiation at one of the resonant frequencies of the coronal plasma. Interferometric measurements (Wild, Sheridan, and Neylan, 1959; Malitson and Erickson, 1966) have since confirmed that the radiation originates from the appropriate plasma frequency level in the corona, although the distances which were derived have suggested an enhancement over the normal run of coronal electron densities. Such an enhancement has frequently been regarded as being due to emission from within a coronal streamer (Malitson and Erickson, 1966;

Hartz, 1969).

The mechanism described above completely ignores the effects of magnetic fields, if such are present in the emitting plasma. The validity of such an approach is open to serious question, since strong,localized magnetic fields exist on the sun, and since a solar background field of about 1 gauss is always present. The coronal streamer models now being constructed by Pneuman (1968, 1969) and others indicate that fields within streamers may be weak or absent. If these models prove to be correct and if it can be directly established by high-resolution observations that Type III bursts do originate in streamers, the neglect of magnetic field effects will have its justification.

C. Previous Time Profile Studies

The use of solar burst time profiles together with theoretical models for the specification of solar burst parameters has been previously attempted only in a very limited way. The initial results of Williams (1948) and de Jager and van't Veer (1958) indicated that an exponential law could be fitted to the trailing position of the profile. Such an approach was later applied by Elgaröy (Elgaröy & Rödberg, 1963; Elgaröy, 1965) to deduce the natural bandwidths of bursts occurring around 200 MHz. Weiss and Wild (1964) approached the problem in a different way; they injected different electron distributions into the corona along

a magnetically neutral sheet and compared the resulting spatial distributions with solar burst time profiles. It had been recognized by Hughes and Harkness (1963) that the lifetime of a burst would depend not only on the operating damping mechanism, but also on the electron spatial distribution. They were unable, however to suggest a clear means of separation of the two.

A more comprehensive approach was taken by the author (Graedel, 1969), who attempted to develop a model for solar radio bursts which would include the effects of the natural burst bandwidth, the reception bandwidth of the instrument used for observing the radiation, the spatial and velocity distributions of the electrons, and the collisional damping of the plasma waves. Although moderately successful, the model was fitted to bursts at only one frequency (3.5 MHz), and this restriction hampered attempts to place stringent limits on the variables involved. Impetus was provided, however, for a model covering a wide range of coronal frequencies; the thinking being that observational comparison of the results of such a model would result in a more comprehensive understanding of the burst phenomena.

II. Formulation of the Problem

A. Mathematical Formulation

The problem of expressing the burst radiation mechanism in mathematical form is complicated by the fact that the unknowns involve both plasma physics and coronal physical properties. A very general mathematical approach is therefore indicated, and such an approach is described below in some detail.

In an ideal treatment of the problem, the insertion of an electron velocity spectrum and a consistant set of coronal characteristics into a theoretical model would yield the output flux density for the burst, as a function of frequency and time. In such a case, for an instantaneous electron velocity spectrum $N_e(r,V)$ a given volume of homogeneous coronal plasma at distance r would produce a plasma wave energy spectrum given by

$$P[f,r] = \int_{V+-\infty}^{V=+\infty} N_e\ (r,V)\ T_1[F(V)]dV, \qquad (1)$$

where $T_1[F(V)]$ is a transfer function expressing the efficiency of the plasma wave production by electrons. The plasma waves

will be damped out by electron-ion collision, Landau damping, and loss of energy due to scattering. The form of the collisional damping is known to be exponential in nature (Jaeger and Westfold, 1949), while that of Landau damping is more complex. As a first order approach, it will be assumed here that the total of the collisional and Landau damping can be expressed by an exponential of the form exp $[-(\Phi_C(\tau)+\Phi_L(\tau))]$, where Φ_C and Φ_L are the appropriate damping constants (see also the discussion on coronal temperature structure), and τ is a time variable. Equation (1) may thus be rewritten as

$$P[f,r,\tau] = e^{-[\Phi_C(\tau)+\Phi_L(\tau)]} \int_{V=-\infty}^{V=+\infty} N_e(r,V) T_1[F(V)]dV \qquad (2)$$

The plasma waves described by equation (2) next scatter off coronal density fluctuations to produce electromagnetic radiation with a frequency spectrum which is presumably affected by the scale size of the density fluctuations, the plasma turbulence, and the strength of any magnetic fields which are present. Refraction and absorption effects will act to damp the radiation. Again, for convenience, an exponential damping is assumed. Thus

$$S[f,r,\tau] = P[f,r,\tau] T_2\left[\frac{dN(v)}{dr}\overline{B}\right] e^{-\Phi_R(\tau)} , \qquad (3)$$

where Φ_R reflects damping due to refraction and absorption.

In the actual case of Type III emission resulting from fast electrons, a spatial dispersion of the electrons will result in extended excitation of the plasma. This may be expressed mathematically by allowing $N_e(r,V)$ to vary also with time. The total plasma wave spectrum is then the sum of the appropriately damped individual wave spectra. Equation (2) becomes

$$P[f, r,t] = \int_{\tau=0}^{\tau=t} e^{-[(\Phi_C+\Phi_L)(t-\tau)]} \left[\int_{V=-\infty}^{V=+\infty} N_e(r,V,\tau)\, T_1[F(V)dV \right] d\tau \quad , \qquad (4)$$

and (3) may be rewritten as

$$S[f,r,t] = P[f,r,t] T_2[\frac{dN(v)}{dr}, \bar{B}] \int_{\tau=0}^{\tau=t} e^{-\Phi_R(t-\tau)} d\tau \qquad (5)$$

At any given time, the radiation received at a radiometer distant from the corona will be the sum of the radiation from all coronal regions. Integrating over r for the volume of interest,

$$S[f,t] = \int_{r=r_1}^{r=r_2} \left[P[f,r,t] T_2[\frac{dN(v)}{dr}, \bar{B}] \left(\int_{\tau=0}^{\tau=t} e^{-\Phi_R(t-\tau)} d\tau \right) \right] dr \; . \qquad (6)$$

Finally, it is necessary to consider the radiometer. If it receives the burst radiation at a center frequency f_c, with a system bandpass of Δf, the received signal is obtained by integrating

equation (6) over this band of frequencies:

$$|S(t)|_{f_c,\Delta f} = \int_{f=f_c-1/2\Delta f}^{f=f_c+1/2\Delta f} \left\{ \int_{r=r_1}^{r=r_2} P[f,r,t] T_2 \left[\frac{dN(v)}{dr}, \bar{B} \right] \left(\int_{\tau=0}^{\tau=t} e^{-\Phi_R(t-\tau)} d\tau \right) \right] dr \right\} df \qquad (7)$$

The specification of the functions contained in equations (4) and (7) is necessary in order to compute the flux density for a given Type III solar burst. The remainder of this chapter will concern itself with the manner in which these functions and the integration limits are specified, and with the techniques of the computation itself.

B. Specification of Parameters

1. Density Structure of the Radio Corona

The coronal density structure is not a simple one, particularly when it is being discussed in connection with solar radio emission. The basic density-structure is that of the "background" or "quiet" corona, which appears to vary over the solar cycle. Macroscopic variations in this structure result from the formation of coronal streamers, plumes, and other enhanced features. Superimposed upon both the background and enhanced corona are small-scale density fluctuations of indefinite scale size. (An excellent summary

of the knowledge of coronal density structures as of 1966 is given by Newkirk (1967)).

The density of the coronal features from which radio burst emission originates seems to have been determined with reasonable accuracy, at least within the range 1 - 3 $R_\odot$ (1 $R_\odot$ is the location of the photospheric surface). As summarized by Malitson and Erickson (1966), interferometric measurements suggest a density structure which is enhanced by a factor of 10 over the background corona, and by a factor of 2 over optically observed streamers. In such an interpretation, it is assumed that radiation occurs principally at the local plasma frequency. It has been suggested that radiation in other resonant frequency modes is possible (Slysh, 1967; Hartz, 1969); electromagnetic waves with frequencies less than the plasma frequency are strongly absorbed, however, and the assumption of radiation at frequencies greater than the plasma frequency merely acts to increase the density discrepancy. The case for emission within a region of enhanced density, and at the local plasma frequency, thus appears to be a strong one.

The density structure of the radio corona past 4 $R_\odot$ is considerably less certain. Zodiacal light photometry and radio source occultation theory provide discordant results, and prompt improvement of this situation does not seem likely. Observations by space probes, however (Ness, Scearce, and Seek, 1963; Neugebauer and Snyder, 1966), have

resulted in density determinations at 1 A.U. Although density enhancements are observed, the frequency of occurrence of solar radio bursts, even at very low frequencies, suggests that an average value is more appropriate for use here.

As a result of the above reasoning, the following densities are thus established for the "radio corona": the Malitson - Erickson values for 1.25 - 4.0 $R_\odot$, and the space probe normal value at 1 A.U. The regions 1.00-1.25 $R_\odot$ and 4.0-125 $R_\odot$ (1 A.U. = 215 $R_\odot$) remain to be specified. For the former, it is of significance that Malville (1967) has noted starting frequencies for Type III bursts of 550-600 MHz during solar maximum. Under the assumption of plasma frequency emission, this implies an electron density of some $4 \times 10^9 cm^{-3}$ in the vicinity of 1.00 $R_\odot$. The approach taken herein is to adopt this value as correct, and to extrapolate the Malitson - Erickson curve to this value in order to specify the 1.00-1.25 $R_\odot$ region.

The "interplanetary" region from 4.0-215 $R_\odot$ demands more drastic assumptions. Since no interferometric data is available for this region (such a measurement requires two widely separated radio astronomy spacecraft experiments), an "informed guess" about the structure is required. The following facts are pertinent to such a determination:

i) The background density structure in this region appears to be adequately satisfied by the theoretical solar wind model of Whang, Liu, and Chang (1966). (This model will be referred to hereafter as the "Whang model.")

ii) The question of how far density enhancements reach out into the corona is an open one, but Tousey (1969) believes 25-30 $R_\odot$ to be about the limit.

iii) Observed drift rates for radio bursts at frequencies below about 5 MHz indicate that an enhanced density structure out to at least 50 $R_\odot$ is required if a constant velocity is to be assumed for the exciting mechanism. Alternatively, a merging of streamer enhanced densities into background densities may be assumed. In this latter case, a decrease in velocity of the exciting mechanism results.

After careful consideration of the above factors, the author is inclined to favor a model which allows decreasing electron velocities. The model chosen is hence one which merges the Malitson - Erickson density value at 4.0 $R_\odot$ into the Whang model at 25 $R_\odot$, and adopts the Whang values thereafter for the 25-215 $R_\odot$ region.

The overall density model, as discussed above, is shown in Figure 1.

It should be noted at this point, and recalled throughout by the reader, that a density model for the radio corona is nothing more than convenient fiction. Even a cursory glance at eclipse photographs is sufficient to reveal the non-uniformity of coronal density structures, and space probe observations at the orbit of the earth suggest that such a situation is not unique to the inner portion of the corona. Any model of the sort described here, therefore, can at best reproduce the average of the observationally-determined values. Since the density model used in these calculations can be changed as desired, however, calculations for different types of models can be (and have been) made. For example, if observations of the variations in burst drift rates and durations over the solar cycle were available, model calculations could be made using density models which attempt to reproduce the solar cycle density variations.

2. Temperature Structure of the Corona

Determinations of the temperature in the low corona have been reasonably consistant in establishing a value over active

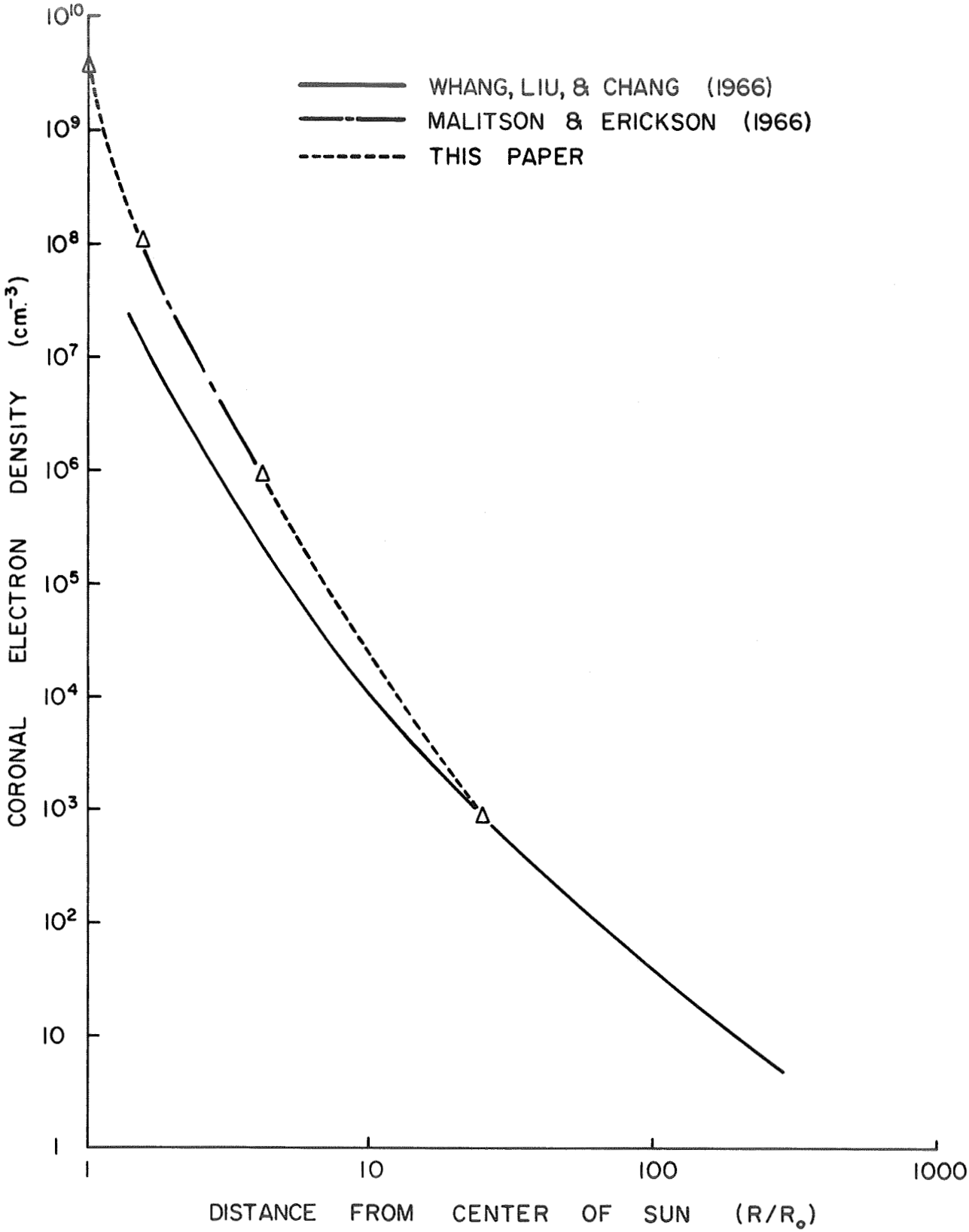

Fig. 1. - Electron density models of the corona.

regions of about 2 x 10^6 °K (Billings, 1966; Newkirk, 1967). The variation of temperature with height has been investigated theoretically by Whang, Liu, and Chang (1966), Scarf and Noble (1965), and others, and inferred from electron density models by Pøttasch (1960). These studies, in combination with space-probe measurements at 1 A.U. (Neugebauer and Snyder, 1966) imply that the mean temperature structure is fairly well determined over the range of distances from the solar surface to the orbit of the earth.

Interferometric measurements of Type III solar burst radiation, and the interpretation of such radiation as emission at the local plasma frequency, have led to the conclusion that solar radio bursts tend to originate from within active region coronal streamers. This point will be analyzed in more detail later in this paper; it is sufficient for this discussion to ask whether the temperature structure of active region streamers differs from that of the background corona. The similarity in density scale-height between the two (Newkirk, 1961; Sturrock and Smith, 1968) argue for a common structure, as do the theoretical streamer studies of Pneuman (1968, 1969). In this paper, therefore, the coronal temperature structure is taken to be identical in both streamer and intrastreamer regions. For convenience, the model adopted is that of Whang, Liu, and Chang (1966) modified slightly so as

to possess a maximum value of 2.0×10^6 °K at the base of the corona.

Estimates of the coronal temperature at distances from low in the corona to nearly 100 R_o have been made from solar radio burst data. The technique is to assume that the plasma oscillations which give rise to the bursts are damped by electron-ion collisions at a rate given by (Jaeger and Westfold, 1949),

$$\Phi_e = 42\, N_e T_e^{-3/2}. \qquad (8)$$

$$\text{Thus,} \quad T_e = 0.65 \times 10^{-4}\, f_p^{4/3} \Delta t^{2/3}, \qquad (9)$$

where Δt is the e-folding time of the burst (Boischot, Lee, and Warwick, 1960). The choice of a coronal density model establishes the plasma frequency height appropriate to the derived temperature. The values resulting from the application of this technique have shown increasing discrepancy from temperatures derived by other methods as more distant coronal regions have been examined, a characteristic which Newkirk (1967) has attempted to explain as being due to unrealistic choices of coronal density models. The most recent work at very low frequencies aboard the satellites Alouette II (Hartz, 1969) and OGO-V (University of Michigan Radio Astronomy Observatory, unpublished), however, gives temperatures for coronal regions at $50 < R/R_\odot < 100$ that are less than those meas-

ured by space probes at 1 A.U. It appears clear that the assumption of plasma wave damping by collisions alone is unsatisfactory, and that additional wave damping mechanisms are operative. In the computations performed herein, therefore, the total wave damping is taken as being given by

$$\Phi_T = \Phi_C + \Phi_L + \Phi_R \qquad (10)$$

where

Φ_T = total damping constant

Φ_C = collisional damping constant

Φ_L = Landau damping constant

and Φ_R = refraction/absorption damping constant

The use of the approach outlined above is simplistic, and is included in this paper as a tractable alternative to a comprehensive theoretical treatment of the wave damping. Its most serious deficiency is that it implicitly assumes that any and all operative damping mechanisms follow an exp $(-\Phi_T t)$ law. While this is almost certainly not correct, it is felt to be a reasonable first attempt toward the solution of the damping problem. The "temperature" model used in this computation refers to the temperature computed by using the best-fit value of Φ_T in equation (9), and is therefore a sort of "effective damping temperature" for the solar radio bursts.

3. Velocity Spectrum of the Injected Electrons

The form of the velocity spectrum of the electrons which are injected into the corona is almost completely unknown. No measurements, of course, have been made at distances substantially closer to the sun than 1 A.U., and even these are not definitive. Current plasma physics theory (Zaitsev and Kaplan, 1966, for example) indicates, however, that the creation of the plasma instabilities which result in plasma wave formation requires a beam of suprathermal electrons. This beam, together with the thermal background, then forms the total plasma velocity distribution. The distribution is unstable if a positive derivative of the quantity $dF(V)/dV$ is present. Such a condition is illustrated in Figure 2.

Some information is available from the frequency drift rates of solar bursts regarding the velocities of the suprathermal electrons. Analyses of the frequency drift rates assume emission at the local plasma frequency, and choose a coronal density model, usually the streamer density model of Newkirk (1961). The rate of drift of the initial impulse with frequency then prescribes a velocity for the electron beam.

The exciter velocities derived using the method outlined above have a fairly large intrinsic range, but their average

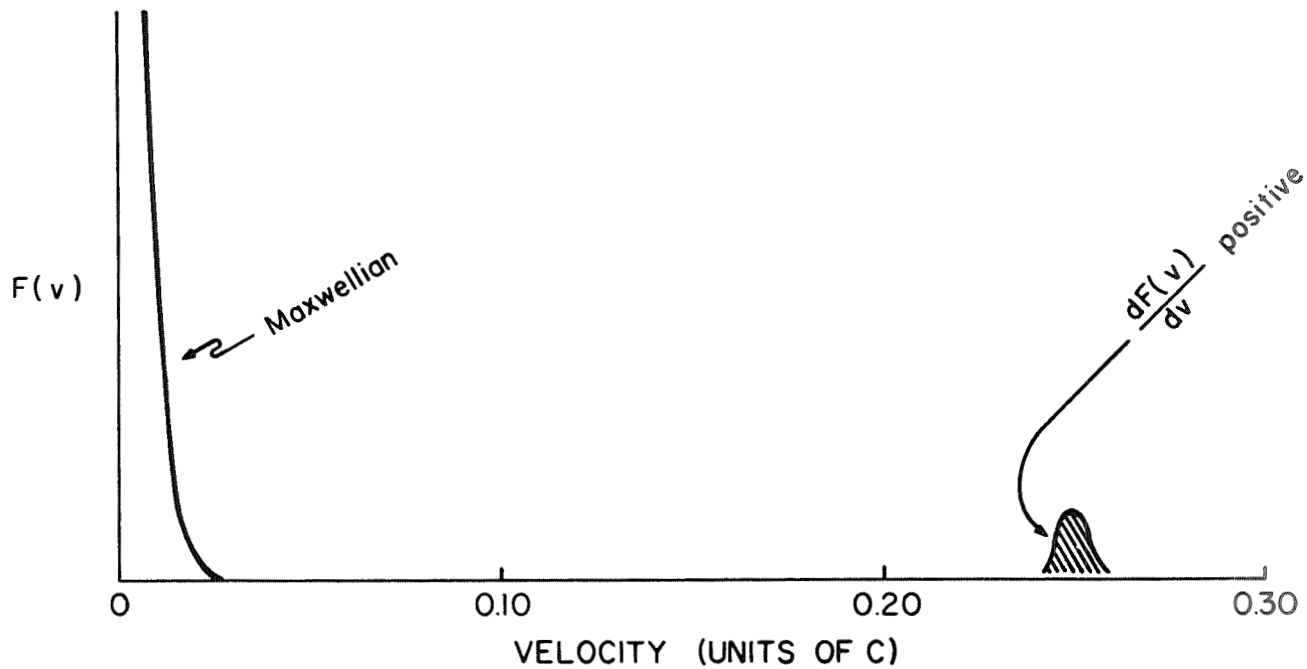

Fig. 2. - An example of the type of unstable electron velocity distribution which produces radiation from a plasma.

values are quite well established, and have been summarized by Graedel (1969) and Hartz (1969). The drift rates themselves are measured values, while their conversion to exciter velocities depends upon the coronal density model chosen. Probably largely for this reason, the resulting velocities show more variation at low frequencies, where the coronal density models are less certain. In the inner corona, the range of velocities is about 0.2 c to 0.6 c, with 0.4 c being an average figure (Malville, 1962). Lower frequency studies have given velocities of 0.1 c to 0.15 c (Hartz, 1964; Slysh, 1967b) and 0.35 c (Hartz, 1969), the difference being due largely to the density model used.

The results outlined above suggest that the average beam of suprathermal electrons has a maximum velocity of 0.35c to 0.4c, which may be constant or may decrease as the beam moves outward into the corona. Although an accelerating process would be expected to provide a spread in velocities, no evidence as to the width of this spread is directly available. The existence of such a velocity dispersion at the photospheric injection point, however, implies a spatial dispersion which becomes increasingly larger with radial distance from the injection point (Hughes and Harkness, 1963; Weiss and Wild, 1964). This spatial dispersion can be computed for a given velocity distribution and provides a means for lengthening the total

durations of Type III bursts.

The velocity spectrum models chosen in this paper are symmetrical, of varying velocity spread, and have maximum velocities in the range 0.18 - 0.60c.

4. Plasma Parameters

The physical mechanisms acting to produce Type III bursts are not well understood, and have not yet been described adequately from a theoretical point of view. It appears that the electron velocity spectrum may be estimated satisfactorily (see the previous discussion), and that the specification of ambient coronal conditions plus the velocity spectrum is sufficient to compute the plasma wave spectrum. Production of electromagnetic radiation then requires the plasma waves to undergo scattering from density fluctuations. The fluctuations are apparently of two types, one being the ion wave density fluctuations formed as a part of the response of the plasma to the electron beam and the second being the macroscopic density fluctuations which are observed in radio source occultation data. Neither density gradient is accurately specified, and the wave response to the effects of the fluctuations is not known.

The electromagnetic radiation produced by the scattering process must next propagate through the inhomogeneous coronal plasma. Although it is apparent that radiation at frequencies below the plasma frequency will not propagate, other effects are less certain. In particular, the propagation angles have been indeterminate, except that on occasion radiation is received from solar bursts occurring on the limb of the sun, thus indicating radiation into a hemisphere. The electromagnetic wave propagation would almost certainly be influenced by the presence of a magnetic field, and, although the strengths of coronal magnetic fields are open to question, fields are almost certainly present.

The purpose of the above discussion is to demonstrate the complexity of the problem, and to point out the unknown factors which would make a detailed theoretical treatment of solar burst mechanisms extremely difficult. The approach adopted here is to separate those parts of the problem which can be specified readily, and treat the remaining functions as a single lumped parameter which is regarded as a variable.

To accomplish the separation, the transfer function in equation (1) is redefined as follows:

$$T_1[F(V)] \equiv T_{1A}[F(V)] \cdot T_{1(\Delta B)} \quad , \qquad (11)$$

where the first factor is the plasma wave amplitude transfer function and the second factor is the plasma wave bandwidth factor.

The bandwidth factor is described in the general case by plasma physics theory. Malville (1962) has computed this factor for plasma waves, both for natural band widths and those imposed by Landau damping. He finds natural bandwidths of .03-.04 f_c at 25 MHz, and notes that density fluctuations of $\Delta N_e/N_e > 0.06$ would increase this figure. In the computations performed here, the bandwidth factor has been varied over the range 0.03 f_p to 0.40 f_p.

A lumped transfer function is now defined by

$$T[F(V),\frac{dN(v)}{dr},\bar{B}] \equiv T_{1A}[F(V)] \cdot T_2[\frac{dN(v)}{dr},\bar{B}] \qquad (12)$$

and set equal to the following:

$$T[F(V)_1 \frac{dN(V)}{dr_1} \bar{B}] \equiv K(V)^x \qquad (13)$$

where K is an unknown constant, V is the velocity of the fast electrons producing the burst, and x is a parameter which may be varied during computation.

Equation (13) represents the major assumption in this work, since it assumes that the sum of the plasma processes producing the observed radiation can be represented by an ex-

tremely simple expression for the electron velocity. The validity of the assumption will be demonstrated by the results of the computations, but such results in no way mitigate the fact that the major operative physical processes are not being treated here in any satisfactory manner.

The form of equations (1) and (13) allow the limits of velocity integration to be easily set, since the computations now deal with fast electrons only. Accordingly, the upper and lower integration limits may be specified by the limits of the injected electron velocity spectrum, which are designated by V_1 and V_2.

With the alterations and redefinitions described above, equation (7) can be rewritten to give

$$|S(t)|_{f_c,\Delta f} = K\int_{\tau=0}^{\tau=t}\left[\int_{f=f_c-\frac{1}{2}\Delta f}^{f=f_c+\frac{1}{2}\Delta f}\left(\int_{r=r_1(fp+\frac{1}{2}T_{1(AB)})}^{r=r_2(fp-\frac{1}{2}T_{1(AB)})}\left\{\int_{V=V_1}^{V=V_2} N_e(r,V,\tau)\cdot V^x dV\right\}dr\right)df\right]e^{-\Phi_T(t-\tau)}d\tau \qquad (14)$$

where the volume of interest is now defined by f_p and $T_{1(AB)}$.

Finally, since K is unknown, and since N_e will be expressed in relative rather than absolute terms, equation (14) is rewritten as a proportionality, and the concession is made that all profiles in time and frequency will be normalized to unity. The final equation for computation is thus

$$|S(t)|_{f_c,\Delta f} \propto \int_{\tau=0}^{\tau=t} \left[\int_{f=f_c-\frac{1}{2}\Delta f}^{f=f_c+\frac{1}{2}\Delta f} \left(\int_{r=r_1(fp+\frac{1}{2}T_{1(AB)})}^{r=r_2(fp-\frac{1}{2}T_{1(AB)})} \left\{ \int_{V=V_1}^{V=V_2} N_e(r,V,\tau)\cdot V^x \cdot dV \right\} dr \right) df \right] e^{-\Phi_T(t-\tau)}\, d\tau. \tag{15}$$

In the work presented here, it has been assumed that the passband of the receiver is small with respect to the observing frequency; hence, the frequency integration has not been performed. Such a computation is easy to include, but adds nothing to the final result unless specific receivers with wide passbands are used for comparison of observational data.

For completeness and convenience, the parameters in equation (13) are defined and described as follows:

$|S(t)|_{f_c,\Delta f}$ = Normalized flux density. This is the final computed electromagnetic flux density as a function of time at a given frequency f_c, for a receiver with passband Δf.

$N_e(V,r,t)$ = Suprathermal electron spectrum. This function gives the number of fast electrons injected per unit time through a unit cross-sectional area of the plasma under study, with the function being normalized to its maximum value. This parameter, together with the bandwidth factor, speci-

fies the volume of the emitting region. The inherent electron velocity dispersion results in variation with distance and time.

$T_{1(\Delta B)}$ = Bandwidth factor. This parameter is expressed as a percentage of f_c, the observing frequency, but refers to the intrinsic plasma wave spectrum bandwidth, rather than to the filtering characteristics of the receiver. The resulting spectrum is taken to be a square wave with

$$\text{Amplitude} = 1 \text{ for } f_p - \tfrac{1}{2} T_{1(AB)} \leq f \leq f_p + \tfrac{1}{2} T_{1(AB)} \quad (16)$$

$$= 0 \text{ elsewhere.}$$

V^x = Variable component of lumped transfer function. The parameter x is designated the "amplitude transfer function."

$e^{-\Phi_T(t-\tau)}$ = Damping term. Φ_T is a function of the ambient temperature, and hence is sensitive to the choice of a coronal temperature model.

III. COMPARISON OF CALCULATIONS WITH OBSERVATIONS

A. Time Profile Behavior as a Function of Parameter Variation

It is possible to vary five separate parameters in the burst profile computations. To assess the problem, therefore, it is appropriate to study the effects of varying one of these factors while holding the remainder constant. Each factor is discussed separately below.

1. Coronal Electron Density Model

This factor has been discussed in detail in the previous chapter, and the choice of an average streamer density model described. Variation of this model changes the derived frequency drift rates somewhat, but not nearly as much as when the suprathermal electron velocity spectrum is varied - a much more likely occurrence. Accordingly, the final density model used in all calculations presented here is that pictured in Figure 1.

2. Wave Damping Model

The decay portion of a time profile, and hence the computed burst lifetime, is strongly dependent on the wave damping model which is chosen. At high frequencies ($f>100MHz$) the time scale of suprathermal electron injection has a major effect on the total duration of the burst, but at all other frequencies the

damping model is the predominant factor. Figure 3 illustrates this effect for computations made with two different temperature models, all other factors being the same. The first computation uses the Whang temperature model and assumes that only collisional damping is present. The second model is one postulated by the author which has much stronger damping. It can be seen that the resulting e-folding durations differ increasingly at lower frequencies, the Whang model giving unrealistic values.

Trial computations of time profiles, particularly at the lower frequencies, have resulted in a damping model which appears to be consistent with observational time profile data. When interpreted according to collisional damping theory, however, the result is quite inconsistent with temperature estimates derived by techniques other than collisional radio burst damping. The collisional form of the damping model, designated "TEG 12", is shown in Figure 4 together with the Whang temperature model and a collisional temperature model by Hartz (1966). Note that extension of the Hartz model to 1 $R_{\odot}$ would give a temperature of the order of 10^7K near the solar surface; this figure is clearly too high (Billings, 1966; Newkirk, 1967). Both the Hartz and TEG 12 models are obviously too low at distances greater than a few solar radii if the Mariner II measurement (Neugebauer and Snyder, 1966) is accepted, and if the assumption of collisional burst damping is retained. More will be said

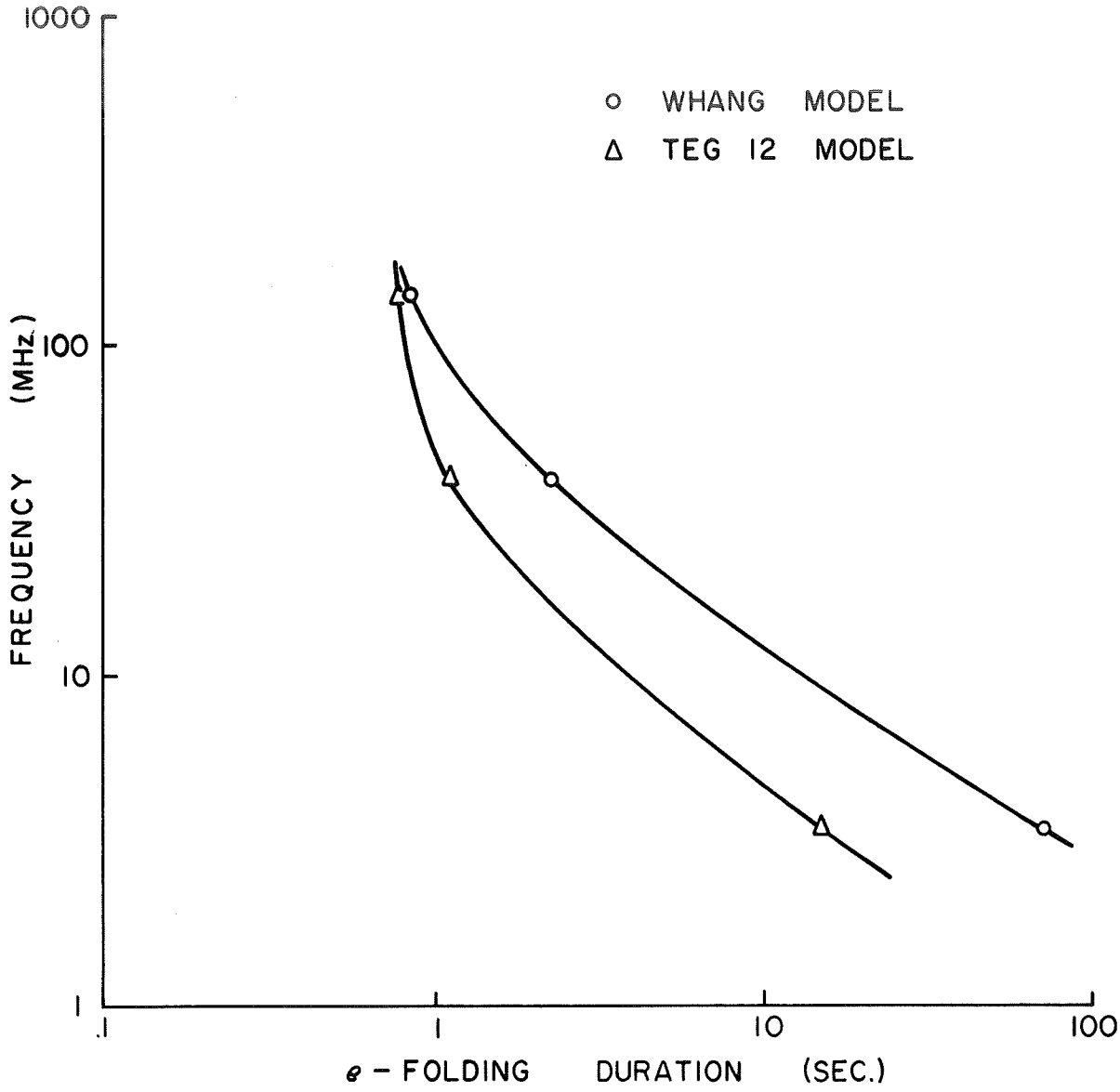

Fig. 3. - The variation in burst lifetimes resulting from computations in which different coronal temperature models are used.

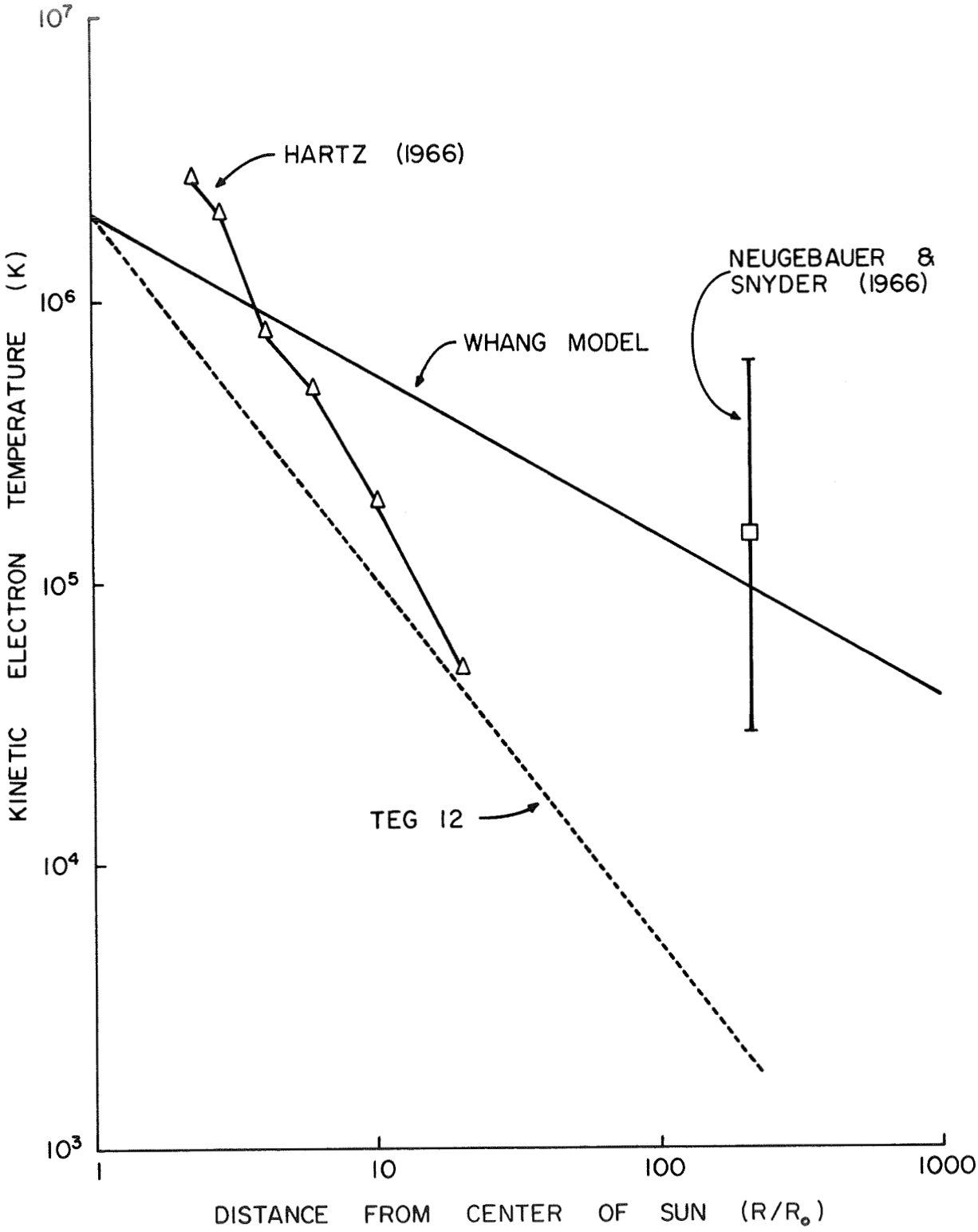

Fig. 4. - Temperature models of the corona.

on these two points later in the paper. Because of its ability to match observed time profiles, however, the TEG 12 model is regarded as conditionally acceptable.

3. Suprathermal Electron Velocity Spectrum Model

Calculations have shown that the model which is chosen for the suprathermal electrons almost totally controls the derived frequency drift rates and has a major effect on the durations of bursts at frequencies above one or two hundred MHz. The former is governed by the highest velocity contained in the velocity distribution, and the latter by the distribution width. Figures 5 and 6 illustrate these effects for computations in which only the electron velocity spectrum was varied.

4. Amplitude Transfer Function

Since all time profiles computed by the method described here are normalized to unity, variatior of the amplitude transfer function affects only the shape of the profile. This is due to the fact that the electrons which first reach a given coronal volume are those with the highest velocities. A large value for the amplitude transfer function thus acts to sharpen the rise portion of the time profile more than does a small value, while having no measureable effect on the burst duration. Figure 7 illustrates profiles computed for f_p=10 MHz, with all parameters except the amplitude transfer function held constant.

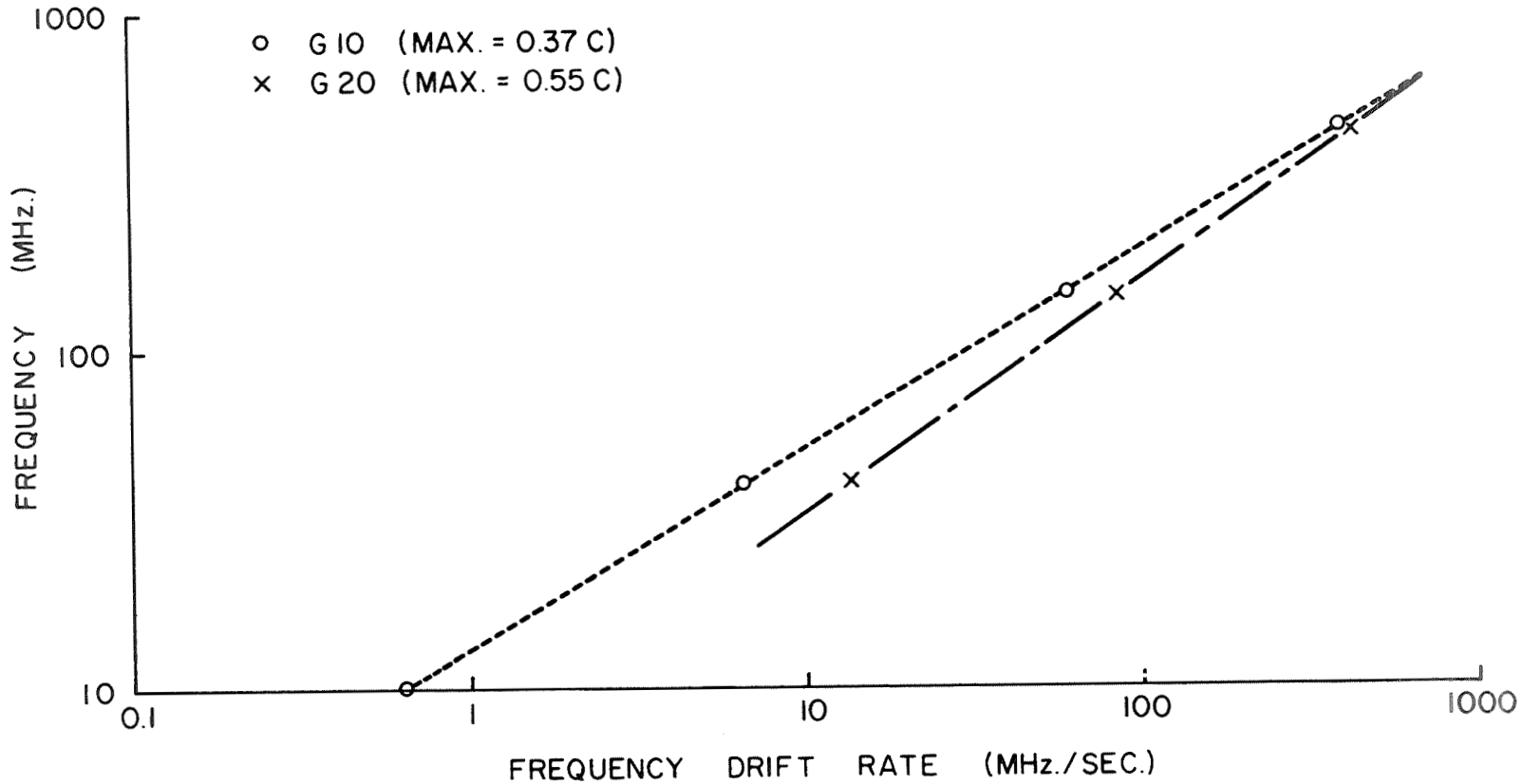

Fig. 5. - Computed frequency drift rates for models in which only the suprathermal electron velocity spectrum is varied.

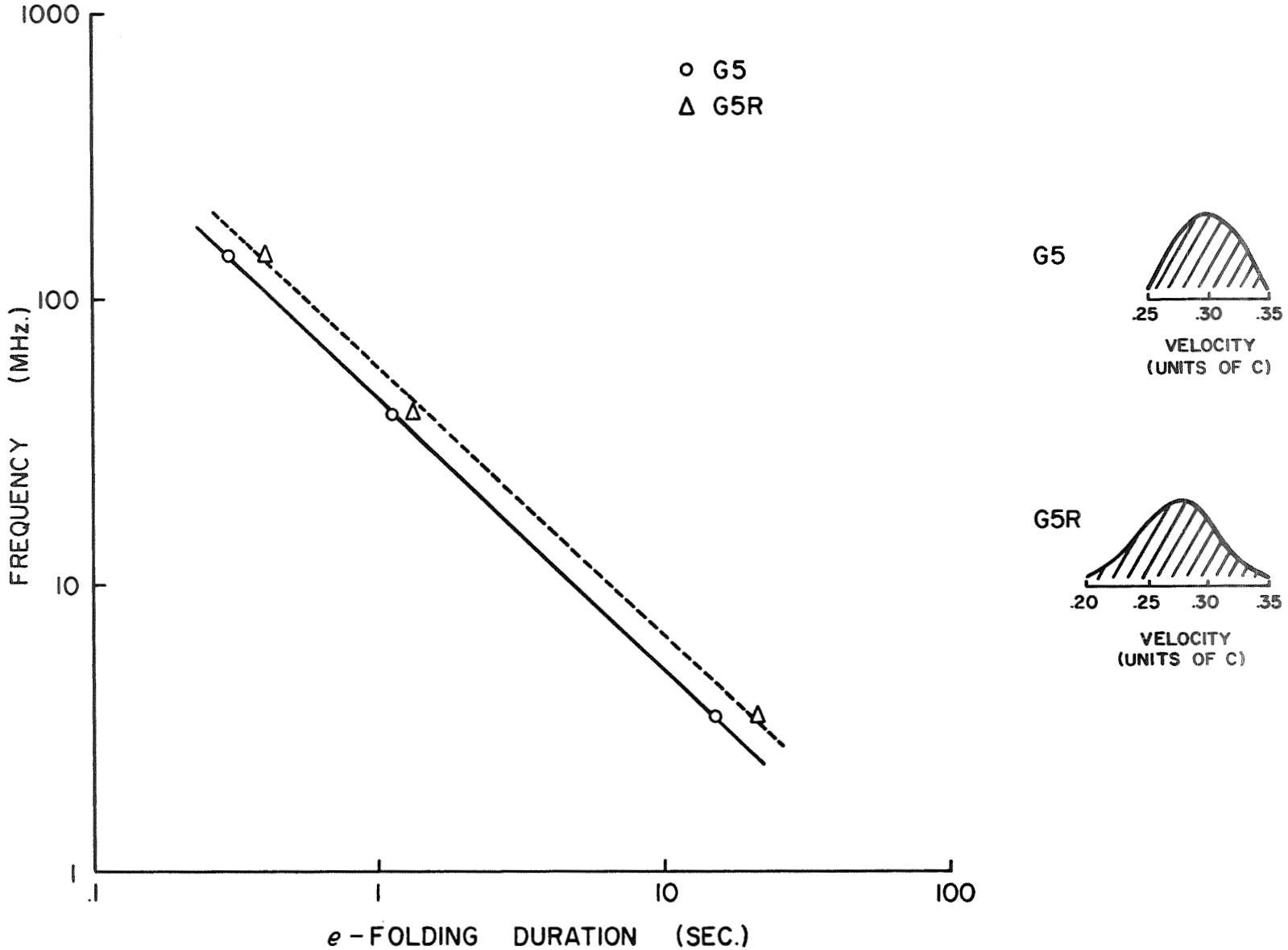

Fig. 6. - The variation in burst lifetime resulting from computations in which different electron velocity spectrum models are used.

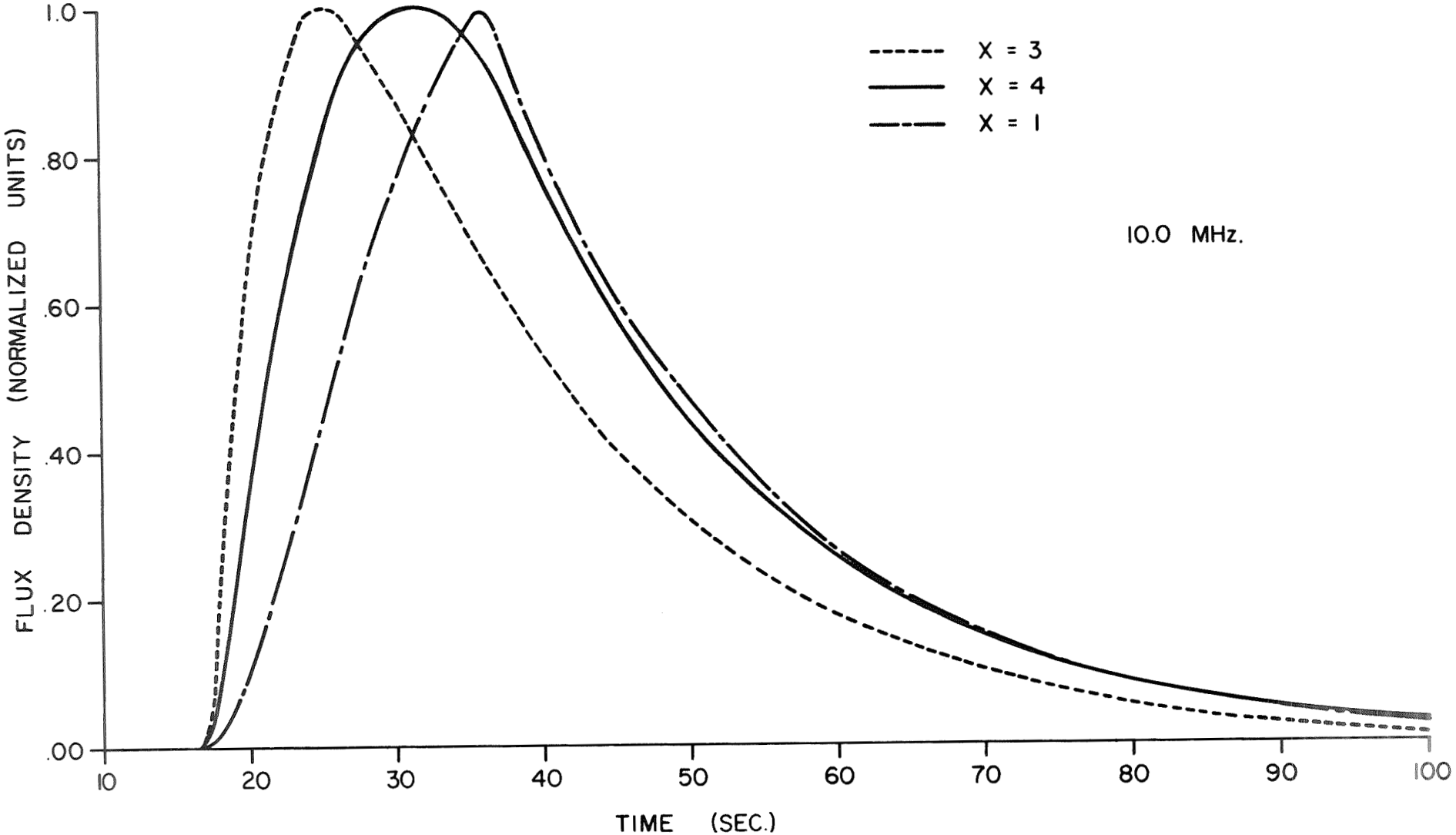

Fig. 7. - The variation in time profiles resulting from computations in which different amplitude transfer functions are used.

5. Bandwidth Factor

The intrinsic bandwidth of the emission determines the volume of the corona from which a radiometer with a discrete passband receives a measureable signal. An increase in the bandwidth factor results in a slower buildup to burst maximum and a slower decay from maximum. As a result of this effect, the total burst duration is influenced, as well as the time profile shape. Only as the bandwidth factor becomes quite large, however ($T_{1(AB)} \geq .25$), is the effect on the profiles significant. Figure 8 illustrates time profiles computed for f_p = 50 MHz, with all parameters except the bandwidth factor held constant.

6. Recapitulation of Time Profile Form Variation

(i) The decay portion of the time profiles is almost completely controlled by the wave damping model used in the computations.

(ii) The frequency drift rates are controlled by the highest velocity of the suprathermal electron model. Burst duration at several hundred Megahertz, where damping and density gradients are both large, is strongly dependent upon the width of the velocity distribution.

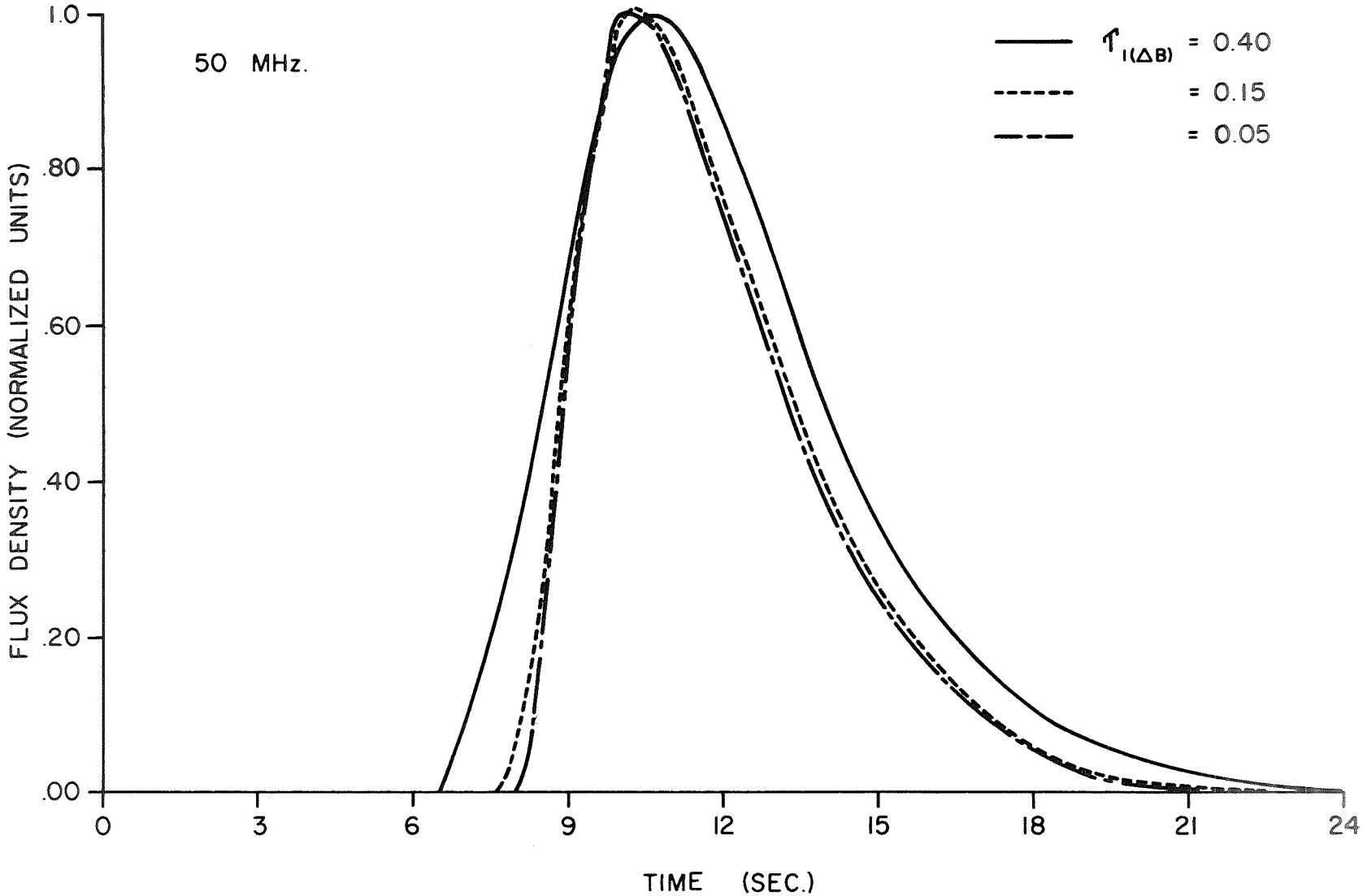

Fig. 8. - The variation in time profiles resulting from computations in which different band width factors are used.

(iii) The amplitude transfer function acts to adjust the profile shape; higher transfer functions tend to produce the rapid rise and quasi-exponential decay which are characteristic of Type III bursts.

(iv) Increasing the bandwidth factor widens the resulting time profile, thus increasing both rise and decay times. The effect is not very significant, however, unless this factor is greater than about 0.25.

B. The Best-Fit Model

Through the use of the computational methods which have been described, series of time profiles at several frequencies were computed for a large number of combinations of the variable parameters, and burst durations and frequency drift rates were derived. The results were then compared with observations for the purpose of selecting the model which best fit the observed characteristics of Type III solar bursts. The model which was chosen as the most suitable has the following characteristics:

(1) The electron density model was that described in Chapter II of this report and illustrated in Figure 1.

(2) The wave damping model was that described in Chapter III and, when interpreted as a collisional damping model, illustrated in Figure 4.

(3) The suprathermal electron velocity spectrum fit the observations only if its velocity was allowed to decrease with distance. It is illustrated in Figure 9.

(4) Model tests of the amplitude transfer function used the values x = 1,4, and 9. The best fit was given for x=9.

(5) The chosen bandwidth factor was $T_{1(AB)} = 0.15$, although the model does not preclude values over the range $0.05 < T_{1(AB)} < 0.20$.

For comparison with observational data, three characteristics of Type III burst were chosen. The first, and most definitive, test, is the comparison of the forms of the time profiles at different frequencies. Only a few of these forms have been observationally determined, since to do so requires an accurate flux density calibration of the radiometer being used. If the radiometer is a sweep-frequency instrument, the calibration problems can be quite difficult. To the author's knowledge, the only time profiles which have been calibrated in intensity or flux density units are at 215 MHz (Elgaroy and Rodberg, 1963),

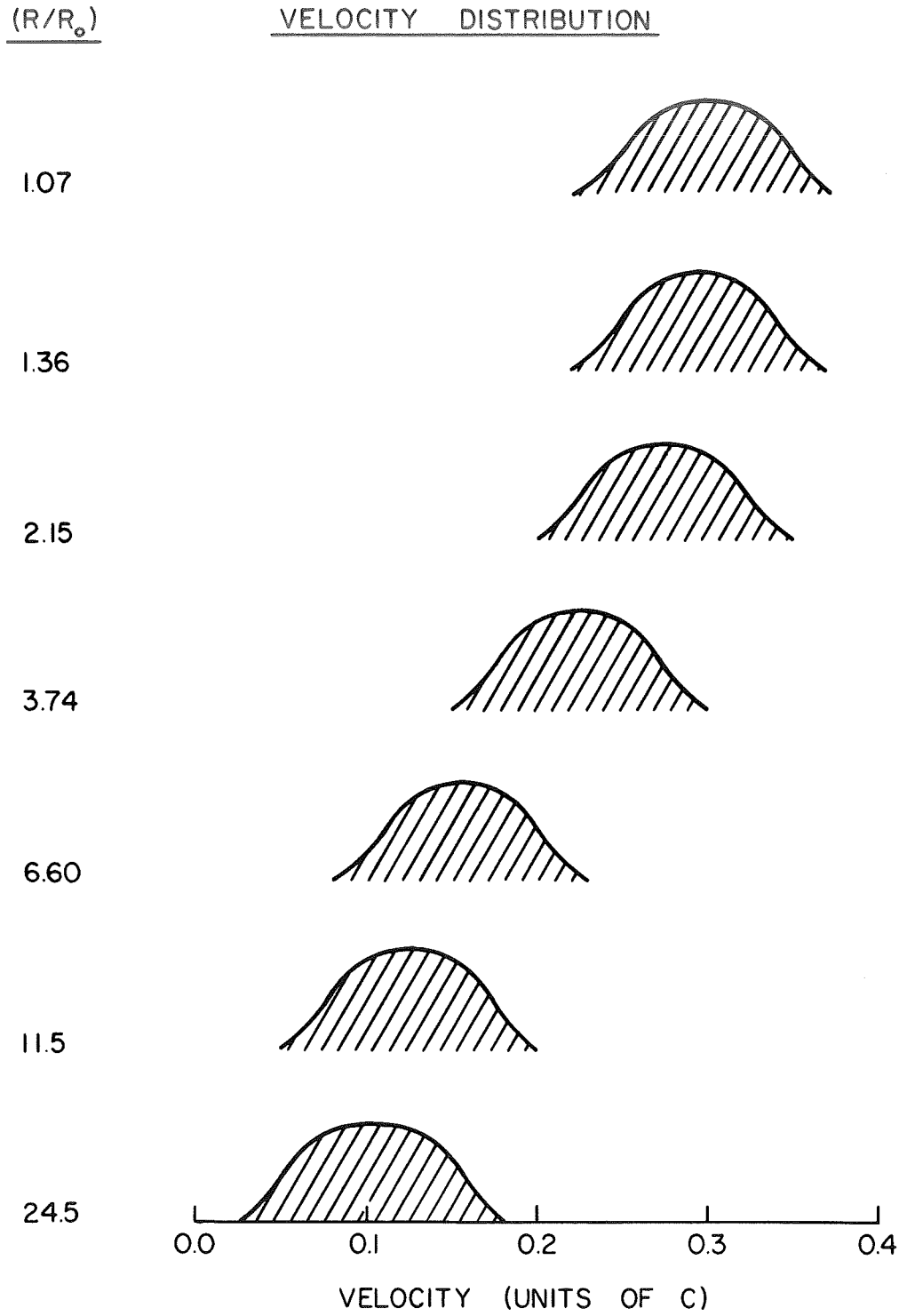

Fig. 9. - Suprathermal electron velocity as a function of radial distance for the best-fit model.

40 MHz (Weiss and Sheridan, 1962), and 3.5 MHz (Graedel, 1969). The profiles are generally slightly asymmetrical, with the decay time being somewhat longer than the rise time. At lower frequencies the longer duration of the bursts increases the time scale; except for this difference the time profiles are quite similar.

Figure 10 compares the time profile computed for 215 MHz using the best-fit model with that observed by Elgaroy and Rodberg (1963). The agreement is very good, differing by no more than a tenth of a second at any point on the profile. In Figure 11, the computed profile for 3.5 MHz is compared with that observed by Graedel (1969). Again the agreement of the same order as for the higher frequency profile.

A second test of theory with observation is provided by a comparison of total burst lifetimes. The observational values are dependent upon detection sensitivity, and it is not always clear whether the given values are half-power durations, e-folding durations, or total observable durations. The general run of the observations form a definite pattern, however, as seen in Figure 12. The line drawn through the points represents a visual fit to the variation of duration with frequency. It is apparent that the computed durations agree very well with observed values over a wide frequency range.

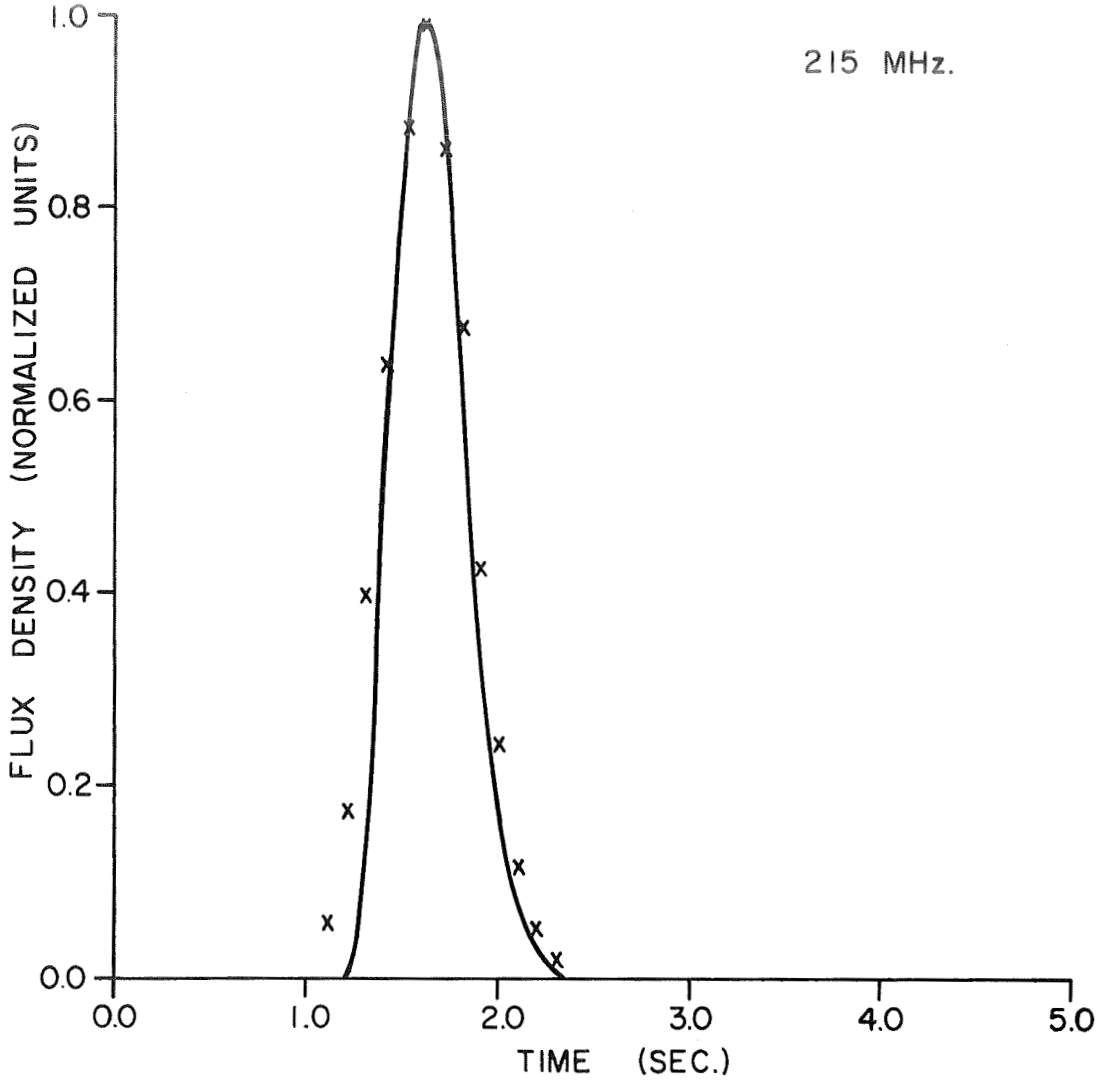

Fig. 10. - Comparison of computed time profile (solid curve) with that observed (x) by Elgaroy and Rodberg (1963) at 215 MHz.

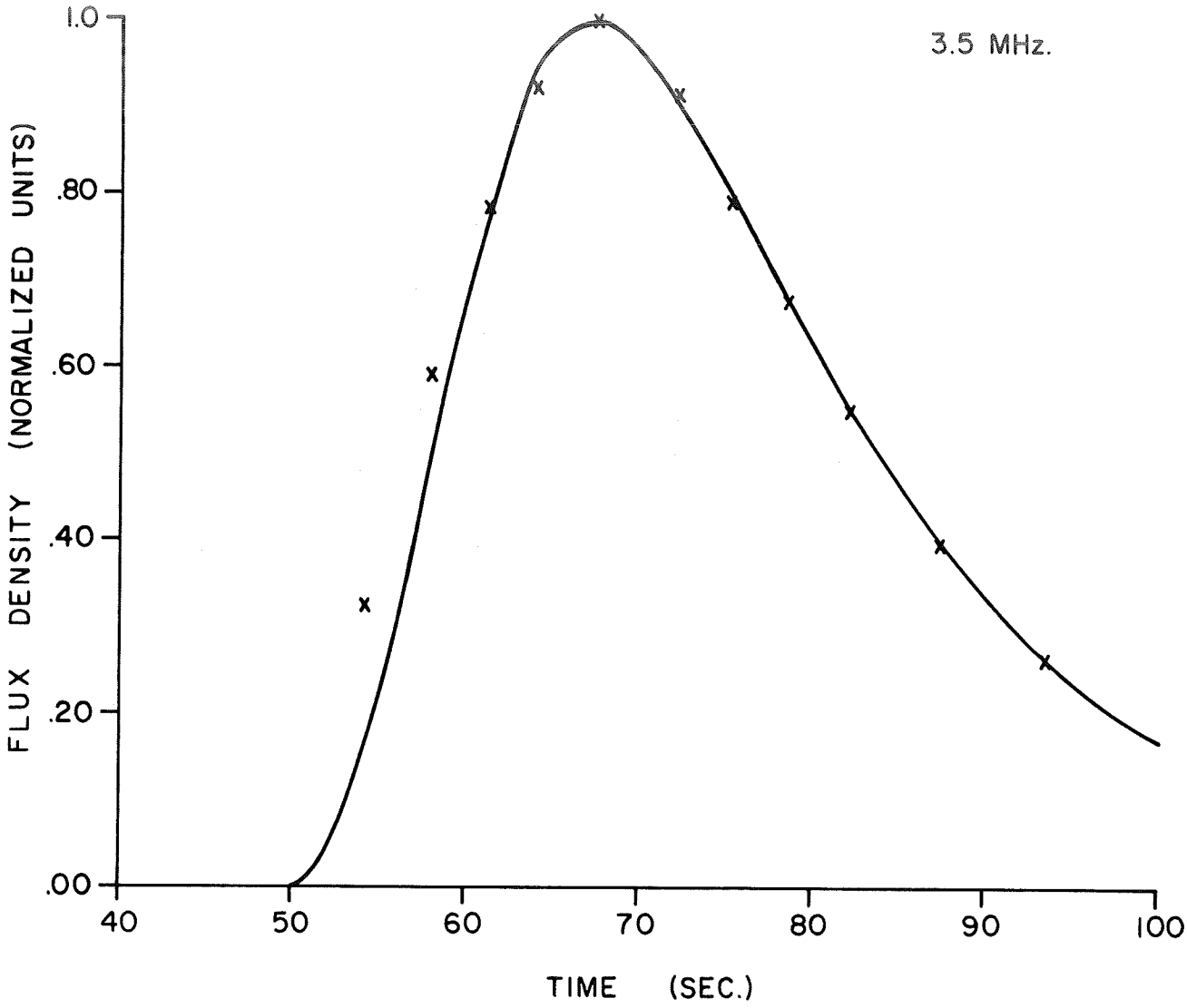

Fig. 11. - Comparison of computed time profile (solid curve) with that observed (x) by Graedel (1969) at 3.5 MHz.

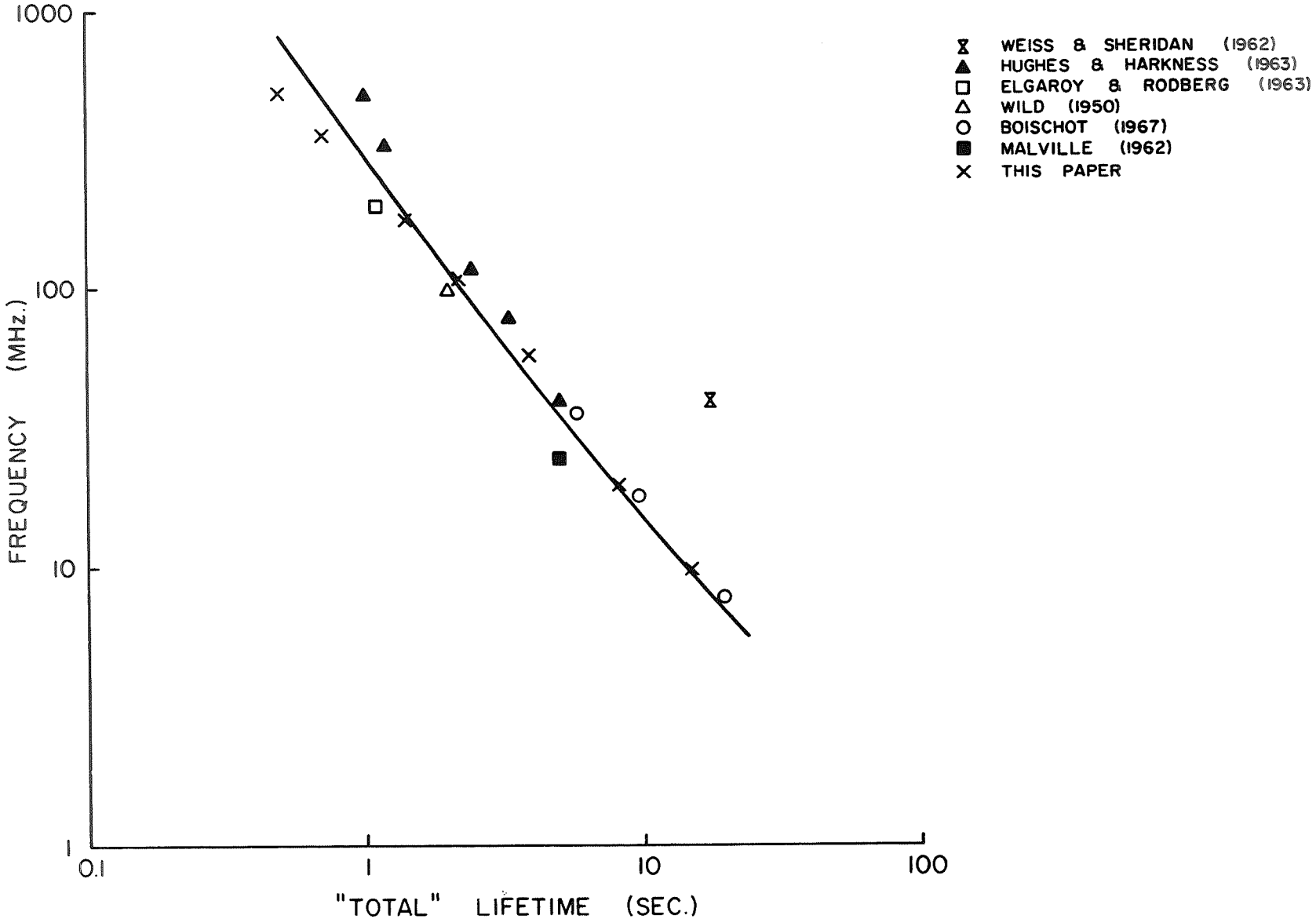

Fig. 12. - Comparison of experimentally determined "total" burst lifetimes with those computed in this paper.

The main differences are between the computed values at frequencies above 300 MHz and the measured values of Hughes and Harkness (1963). It is not readily apparent where the error lies; it should be noted that the time resolution on the observational records, 0.3 seconds, is a substantial fraction of the total burst duration at high frequencies.

The measured duration of Weiss and Sheridan (1962) seems inconsistent with the other duration measurements pictured on Figure 12. Doubt about this value has also been expressed by Elgaroy and Rodberg (1963). It has proved impossible to fit the Weiss and Sheridan time profile and/or duration with any consistent model in this study, and it appears that their intensity calibration cannot be correct.

A final observational test of the model is the observed frequency drift rate behavior as a function of frequency. High-frequency drift rates have been derived by Hughes and Harkness (1963) and low-frequency drift rates by Hartz (1969). The results of these two papers are combined in the solid line on Figure 13. The excellent agreement of the values derived by the model over a wide frequency range constitutes a major argument for its appropriateness.

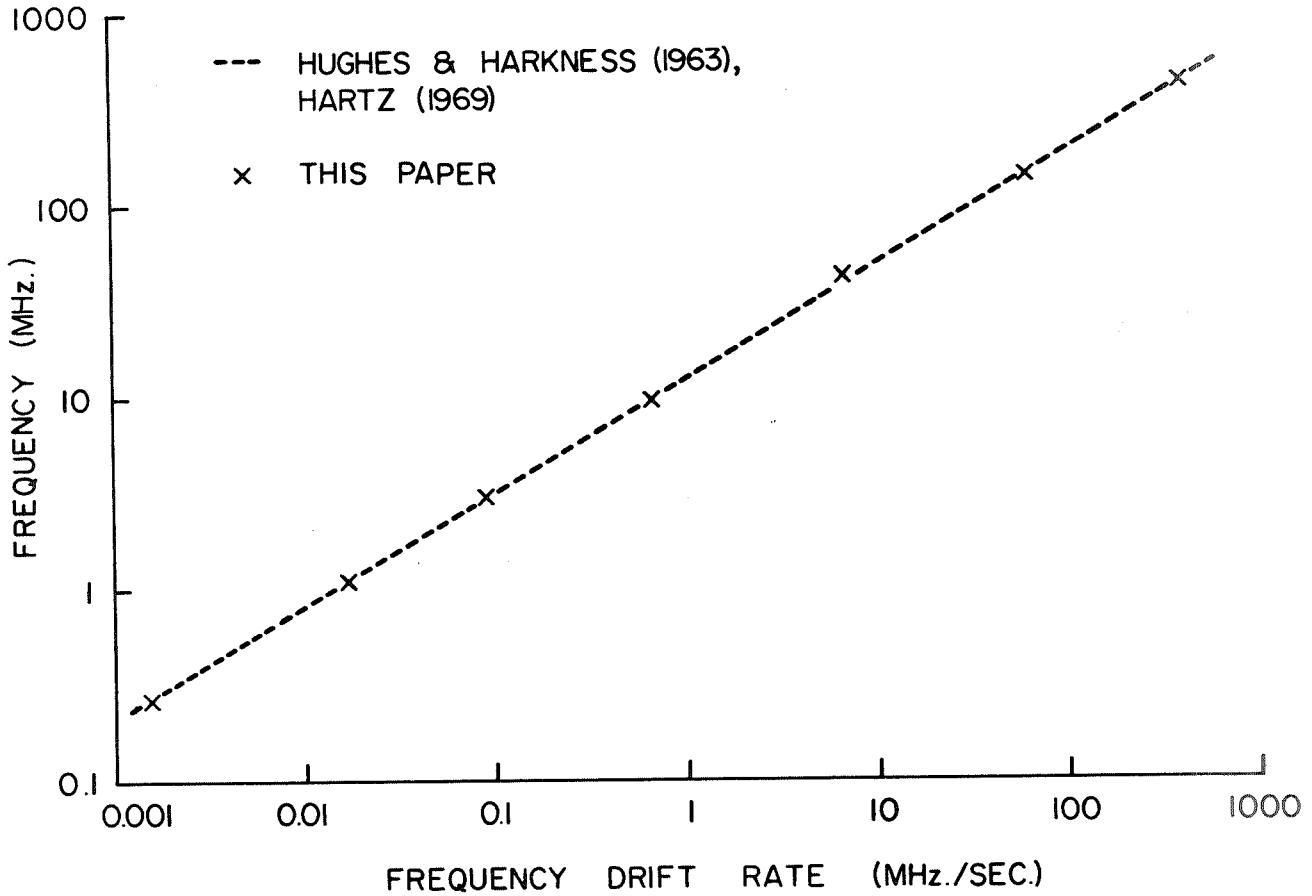

Fig. 13. - Comparison of experimentally determined frequency drift rates with those computed in this paper.

C. Parameters for Computed Time Profiles

In order to allow other observers to make comparisons with the computed time profiles, Figures 14-22 give the results of computations for a number of frequencies, using the final model just described. Table 1 gives some of the properties of these time profiles.

TABLE 1

Properties of Computed Time Profiles

Frequency (MHz)	Δt for Computation (sec)	fp Level ($R/R_\odot$)	Total Duration (sec)	Half-power Duration (sec)	e-folding Duration (sec)
500	0.05	1.04	0.50	0.20	0.12
425	0.05	1.07	0.55	0.23	0.15
350	0.05	1.10	0.70	0.26	0.17
180	0.05	1.28	1.4	0.41	0.27
145	0.05	1.36	1.7	0.55	0.40
110	0.05	1.49	2.2	0.74	0.50
60	0.10	1.85	4.3	1.3	1.0
40	0.10	2.15	5.4	1.6	1.3
20	0.10	2.80	8.2	2.4	1.8

D. Dynamic Spectra of Type III Bursts

It is possible to display dynamic spectra of solar radio bursts in either of two ways. In the first, several time profiles are placed adjacent to each other in such a way that their flux-density modulation (the y-coordinate) assumes a three-dimensional character. The second method is more common; it utilizes intensity

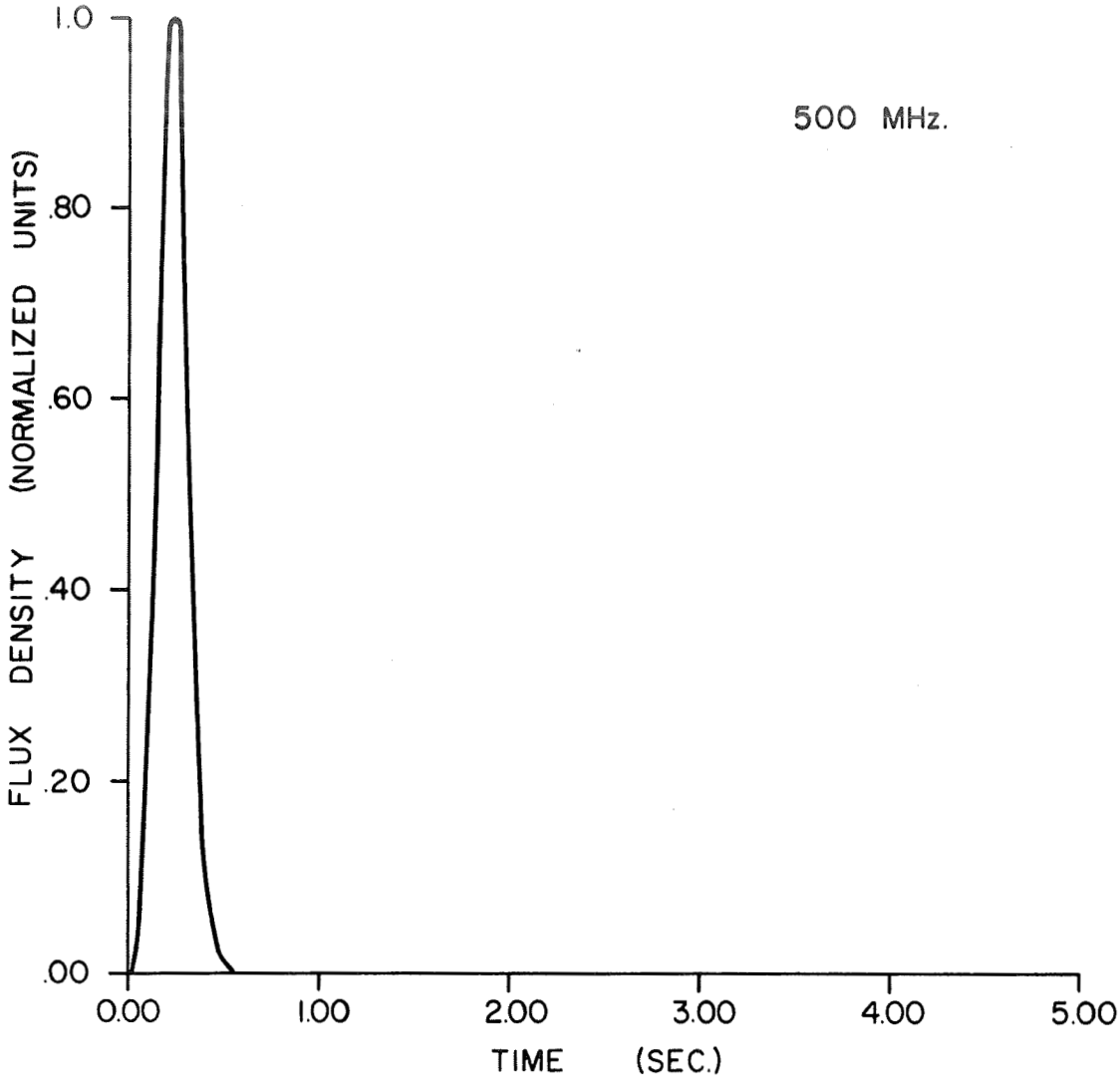

Fig. 14. - Computed time profile for Type III burst at 500 MHz.

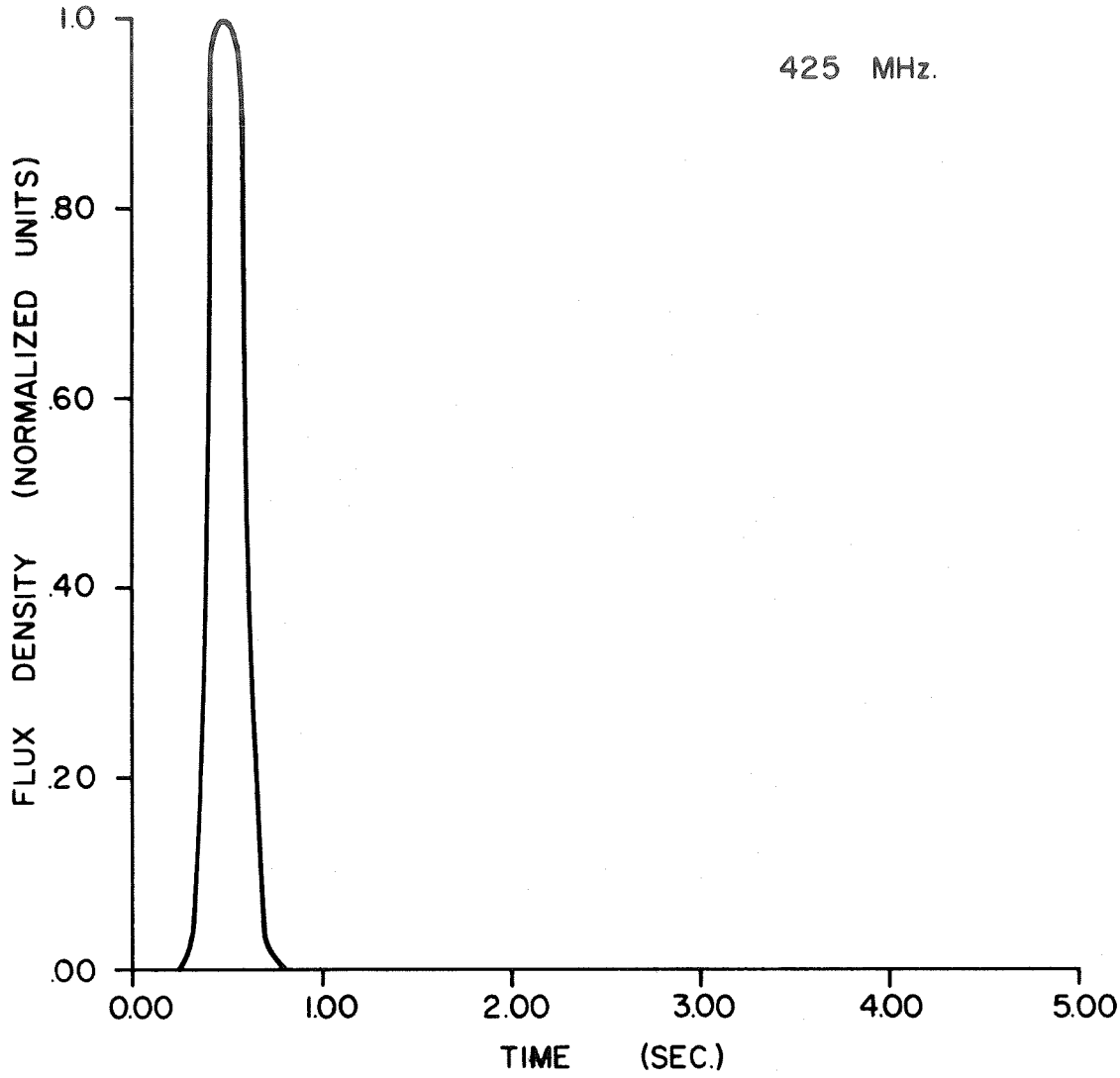

Fig. 15. - Computed time profile for Type III burst at 425 MHz.

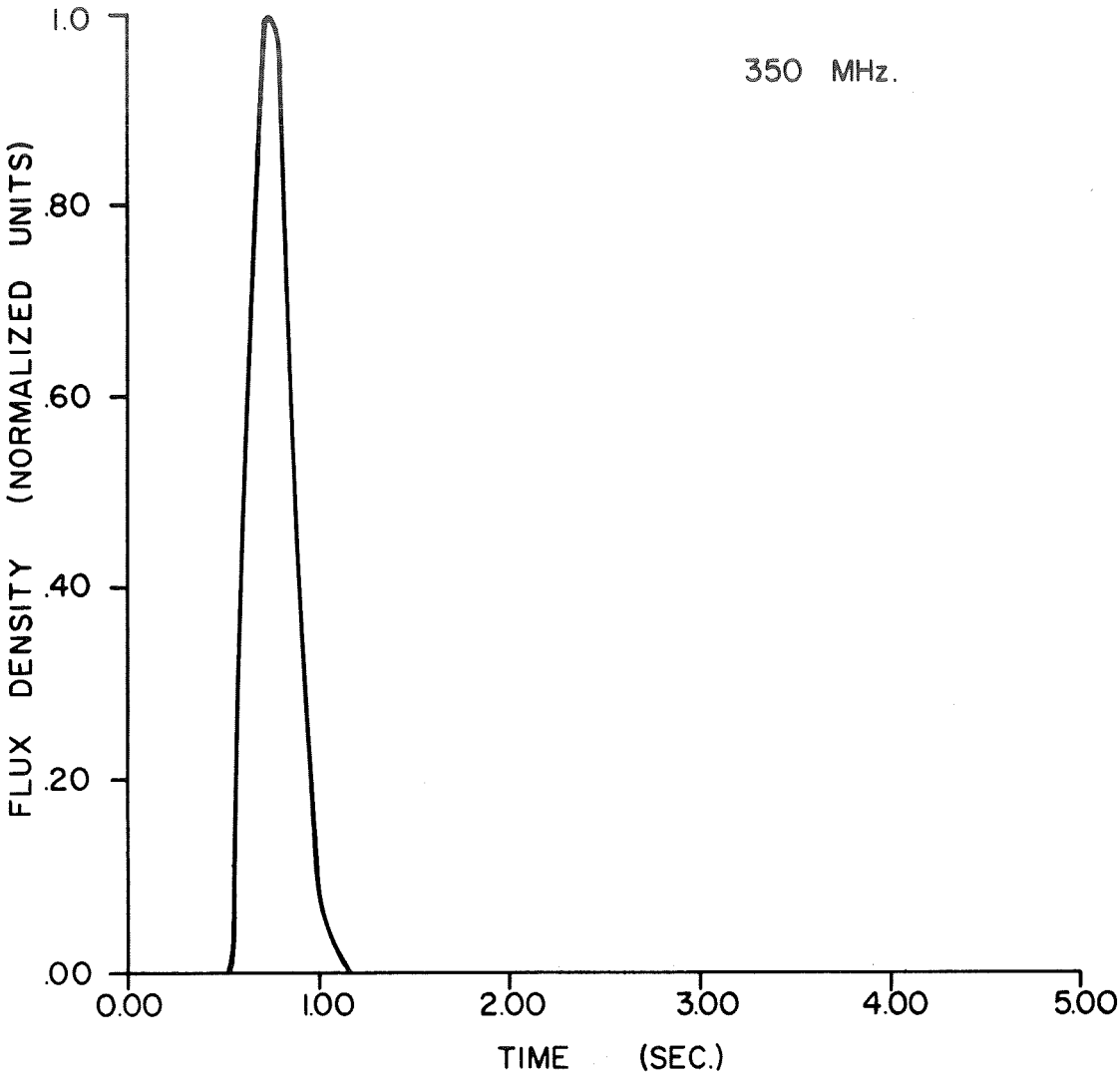

Fig. 16. - Computed time profile for Type III burst at 350 MHz.

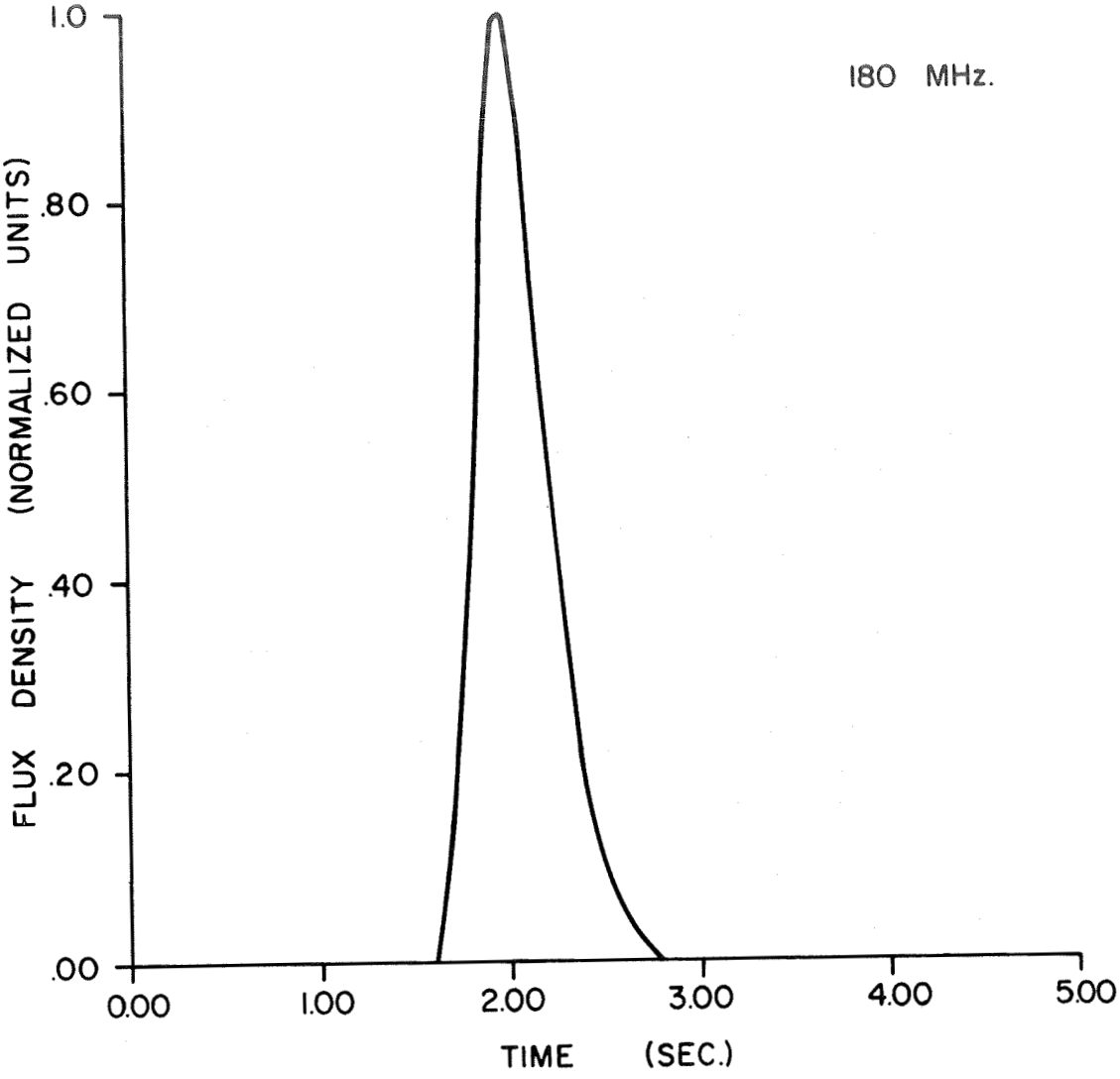

Fig. 17. - Computed time profile for Type III burst at 180 MHz.

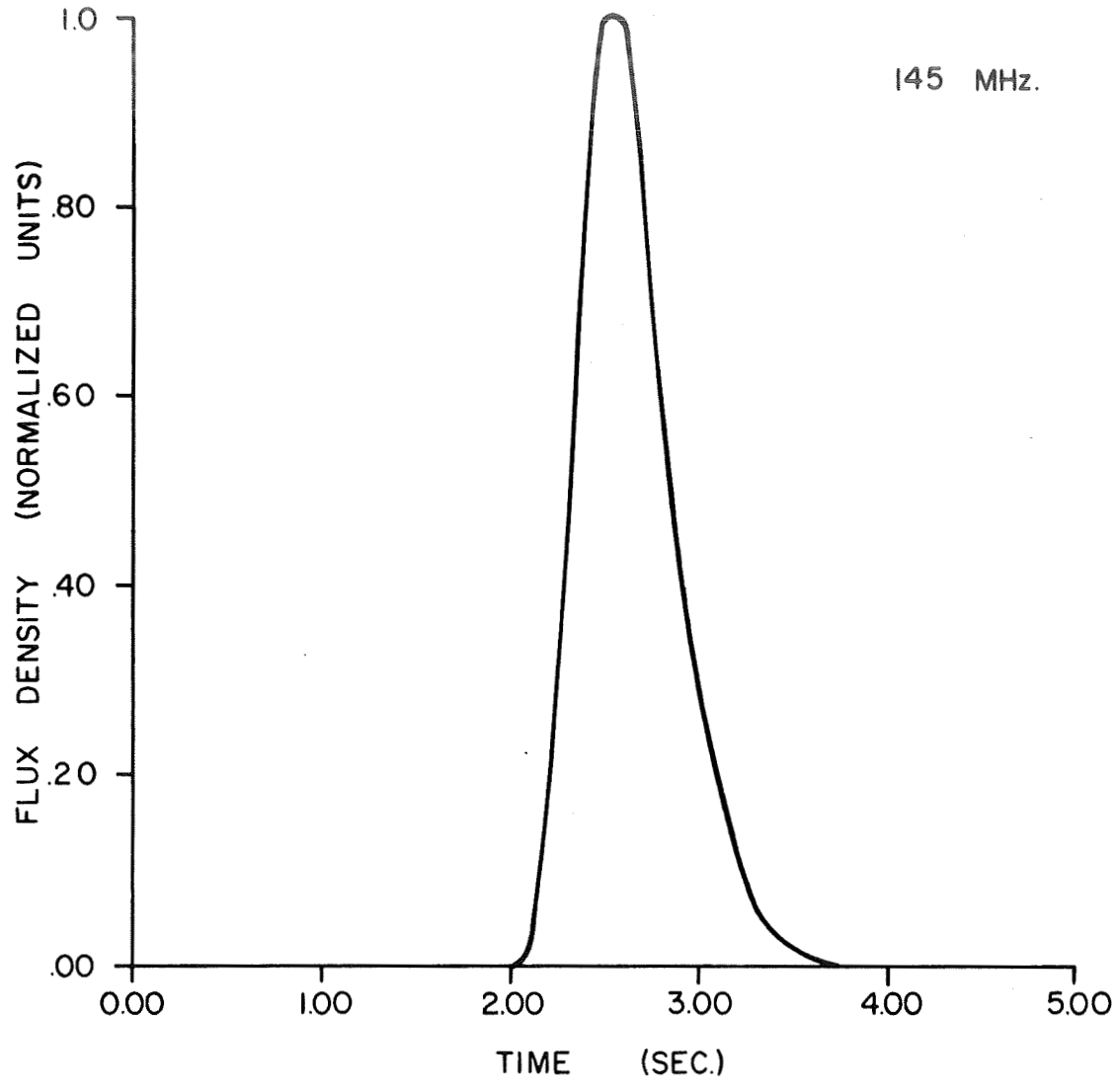

Fig. 18. - Computed time profile for Type III burst at 145 MHz.

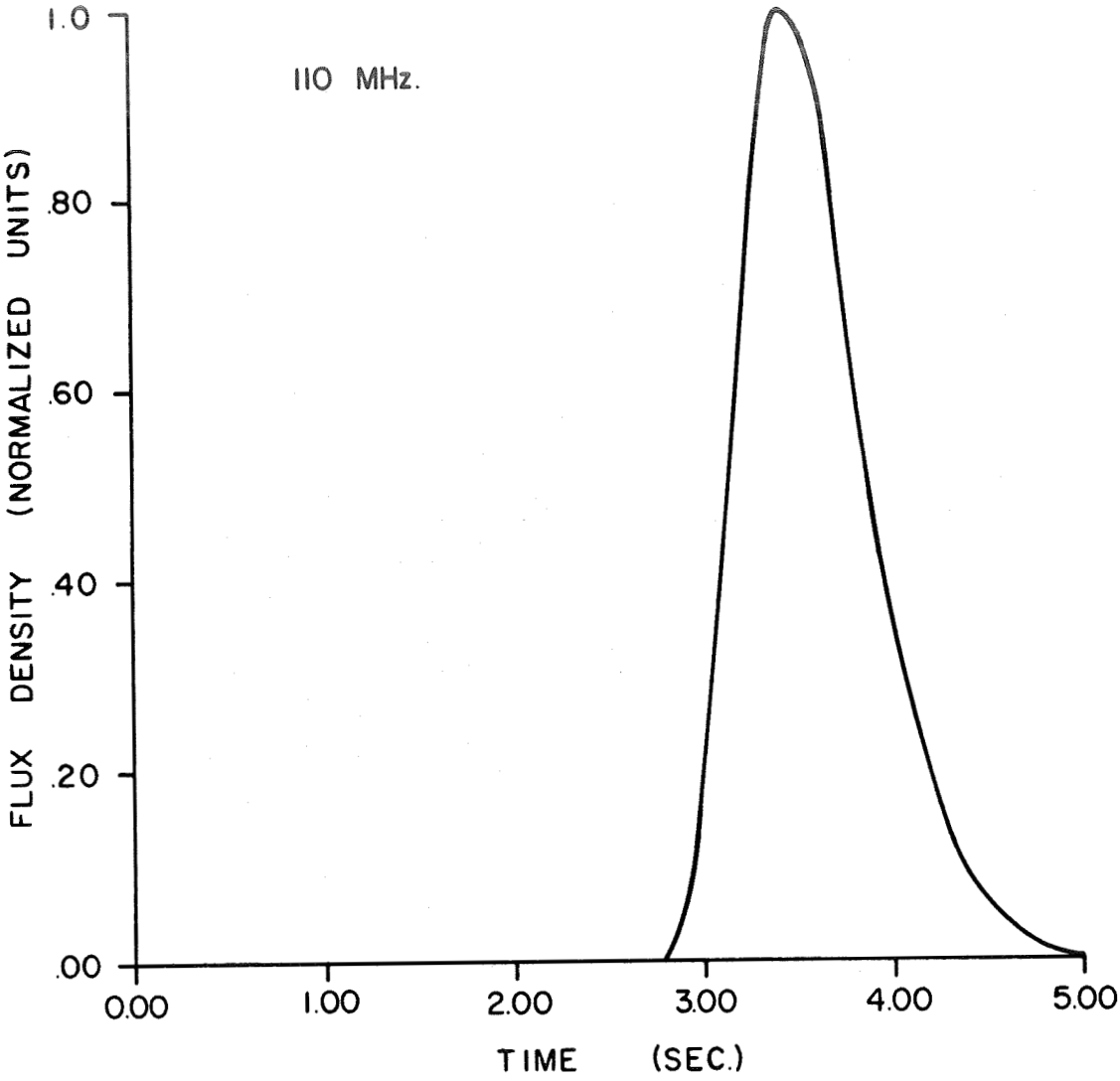

Fig. 19. - Computed time profile for Type III burst at 110 MHz.

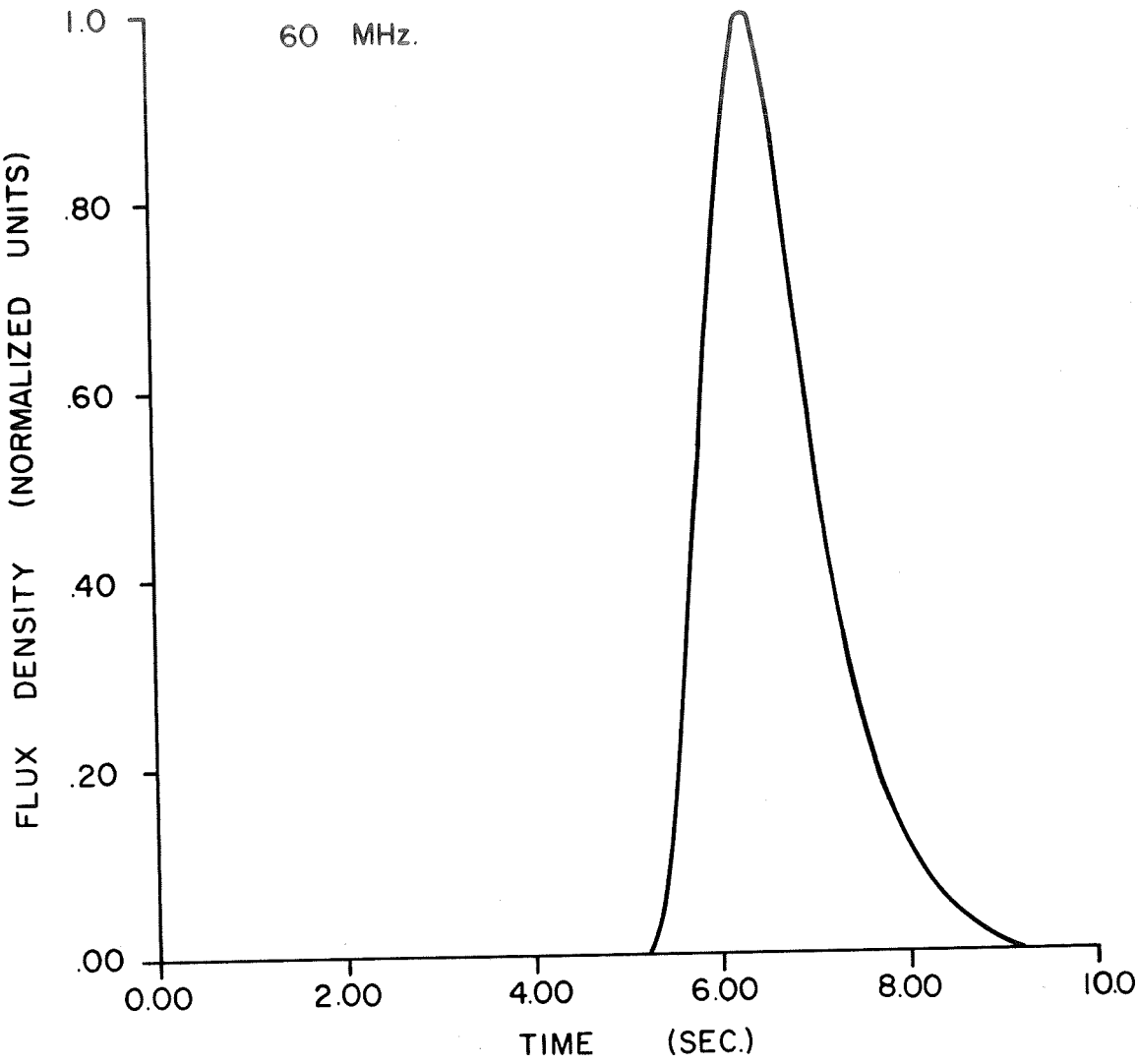

Fig. 20. - Computed time profile for Type III burst at 60 MHz.

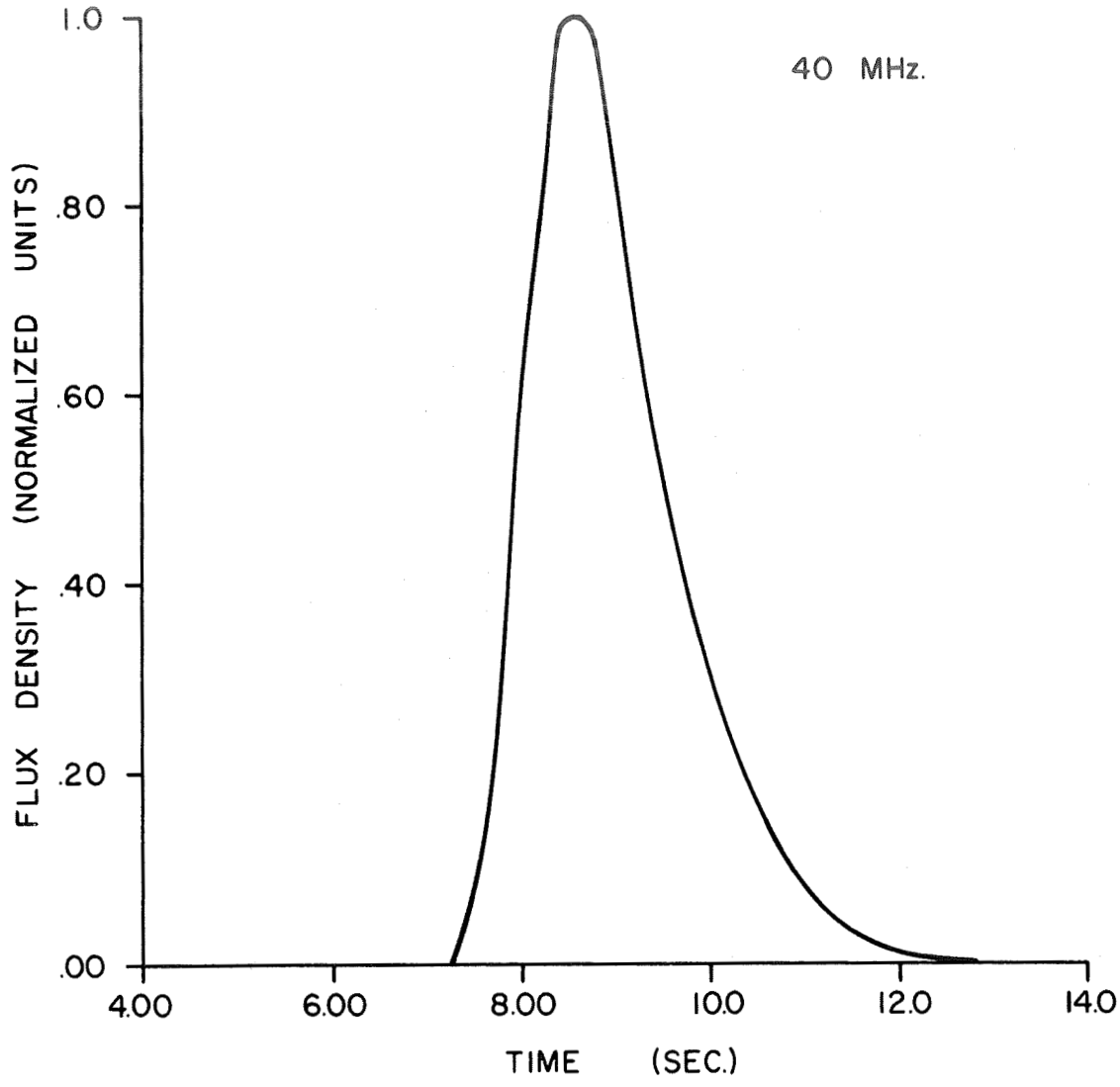

Fig. 21. - Computed time profile for Type III burst at 40 MHz.

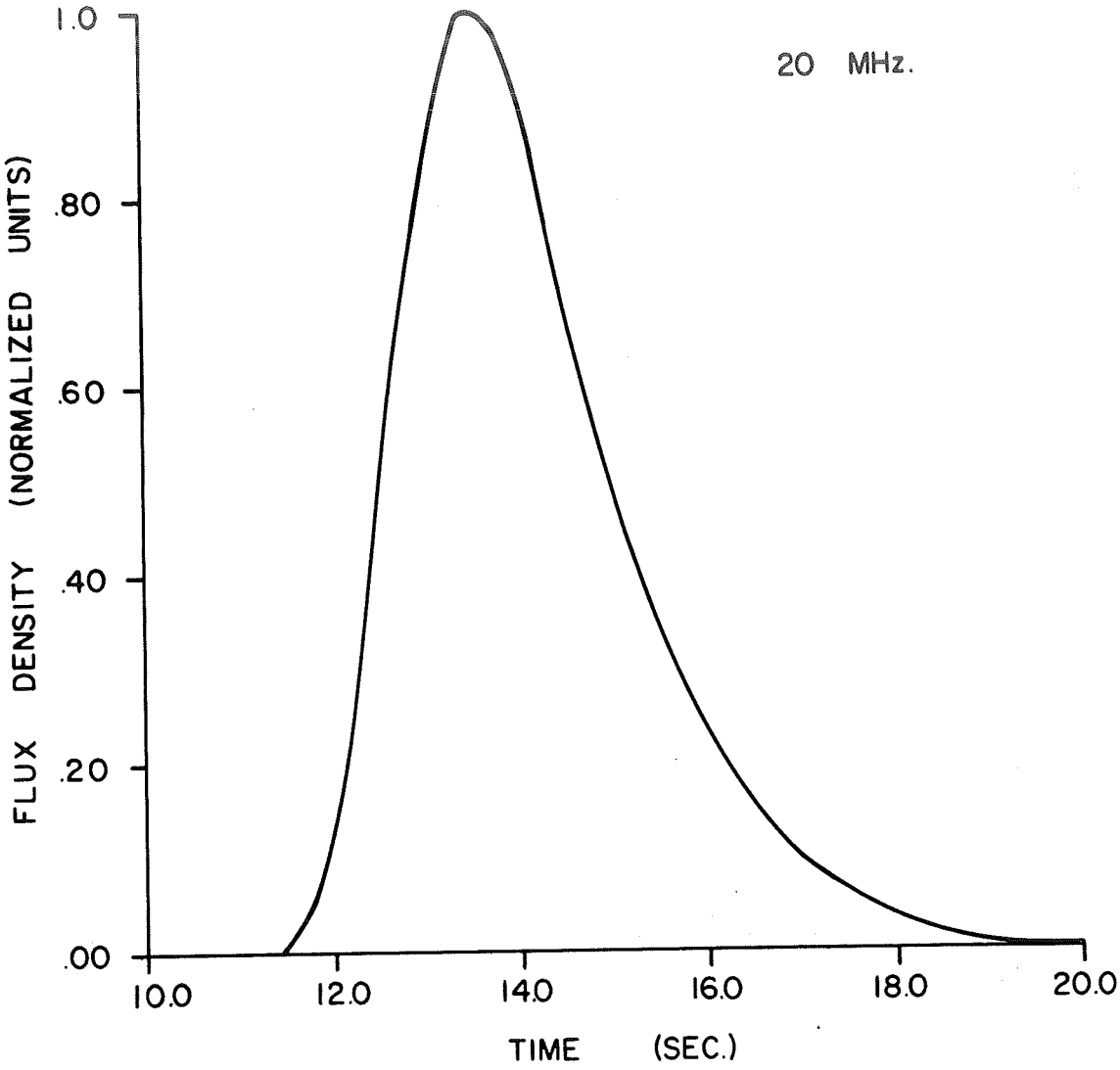

Fig. 22. - Computed time profile for Type III burst at 20 MHz.

variations to express the changes in flux density. In the work described here, a basic set of five time profiles is computed, and the resulting dynamic spectra are then displayed on a CRT and photographed. Figure 23 illustrates the two dynamic spectrum models for a frequency range of 180 to 110 MHz. A more realistic diagram is obtained by interpolating between the five basic time profiles and then displaying both the basic and interpolated values. The resulting dynamic spectra are shown in Figure 24. The multiple bursts which are often seen on spectral records may be readily produced by injecting a time lag into the computations and adding the resulting time profiles to those obtained originally. This technique may be repeated one or more times to produce the dynamic spectra seen in Figure 25 and 26.

Dynamic spectra over different frequency bands and with a variety of time compressions are shown in Figures 27-31. In Figure 32 a double burst at low frequencies is shown, the burst duplicity being clearly evident. Figure 33 demonstrates, however, that when the two bursts occur close together in time it may not be possible to detect the duplicity on the intensity modulated spectrum even though it is visible on the y-axis-modulated spectrum. This result points out the caution needed when interpreting spectral records, measuring durations,etc.

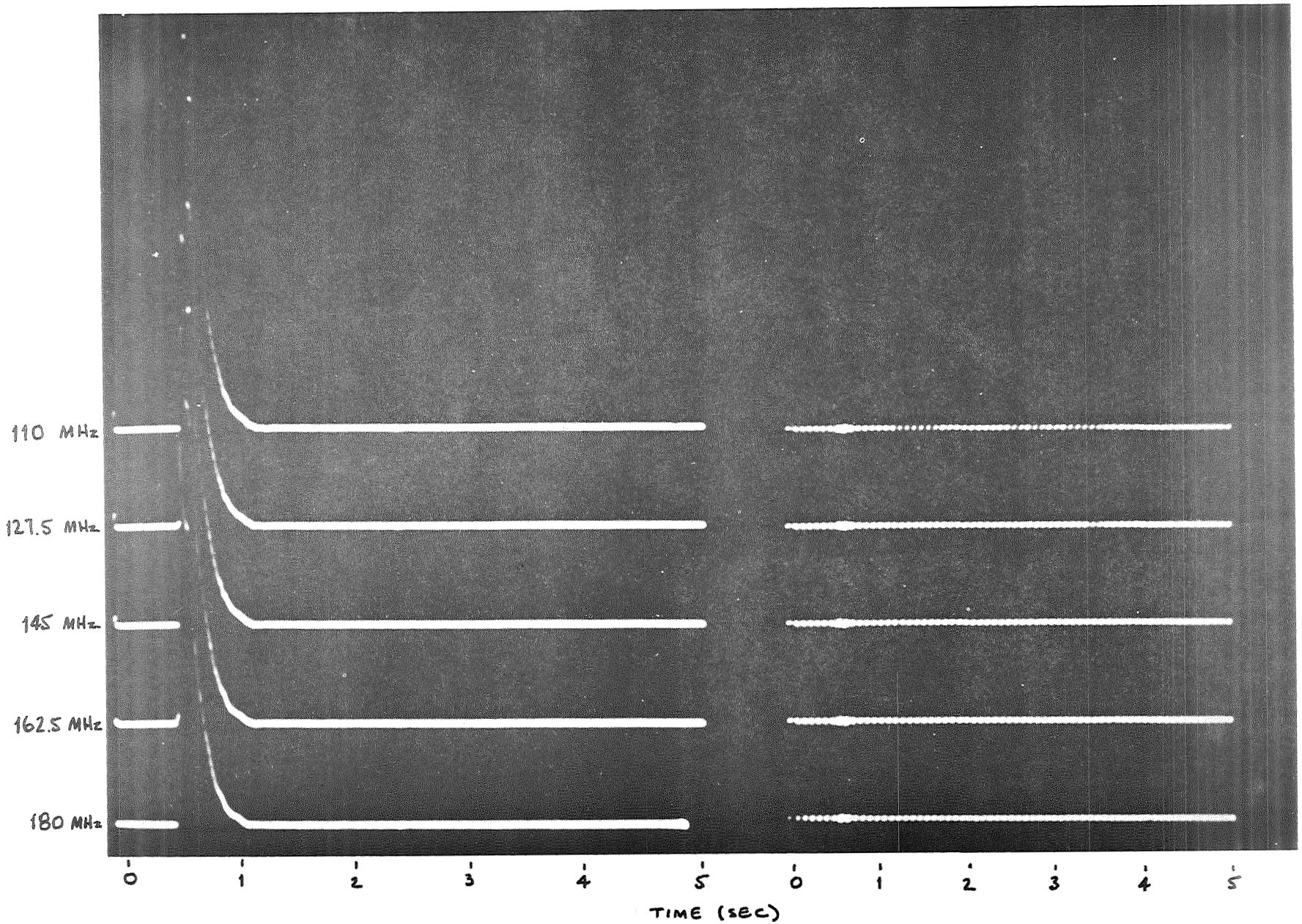

Fig. 23. - Computed dynamic spectrum over the frequency band 180 - 110 MHz.

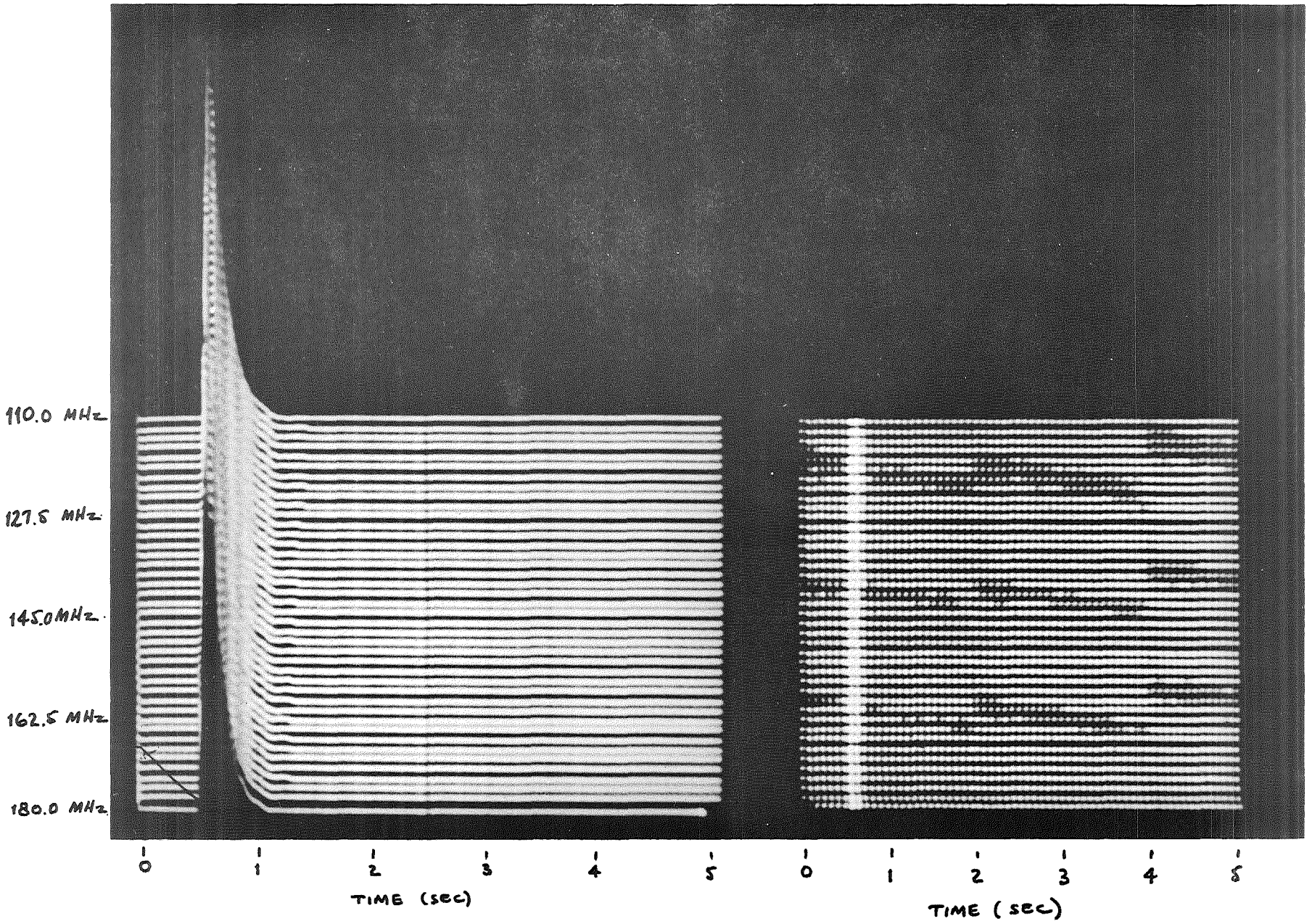

Fig. 24. - Same as Fig. 23, but with interpolation.

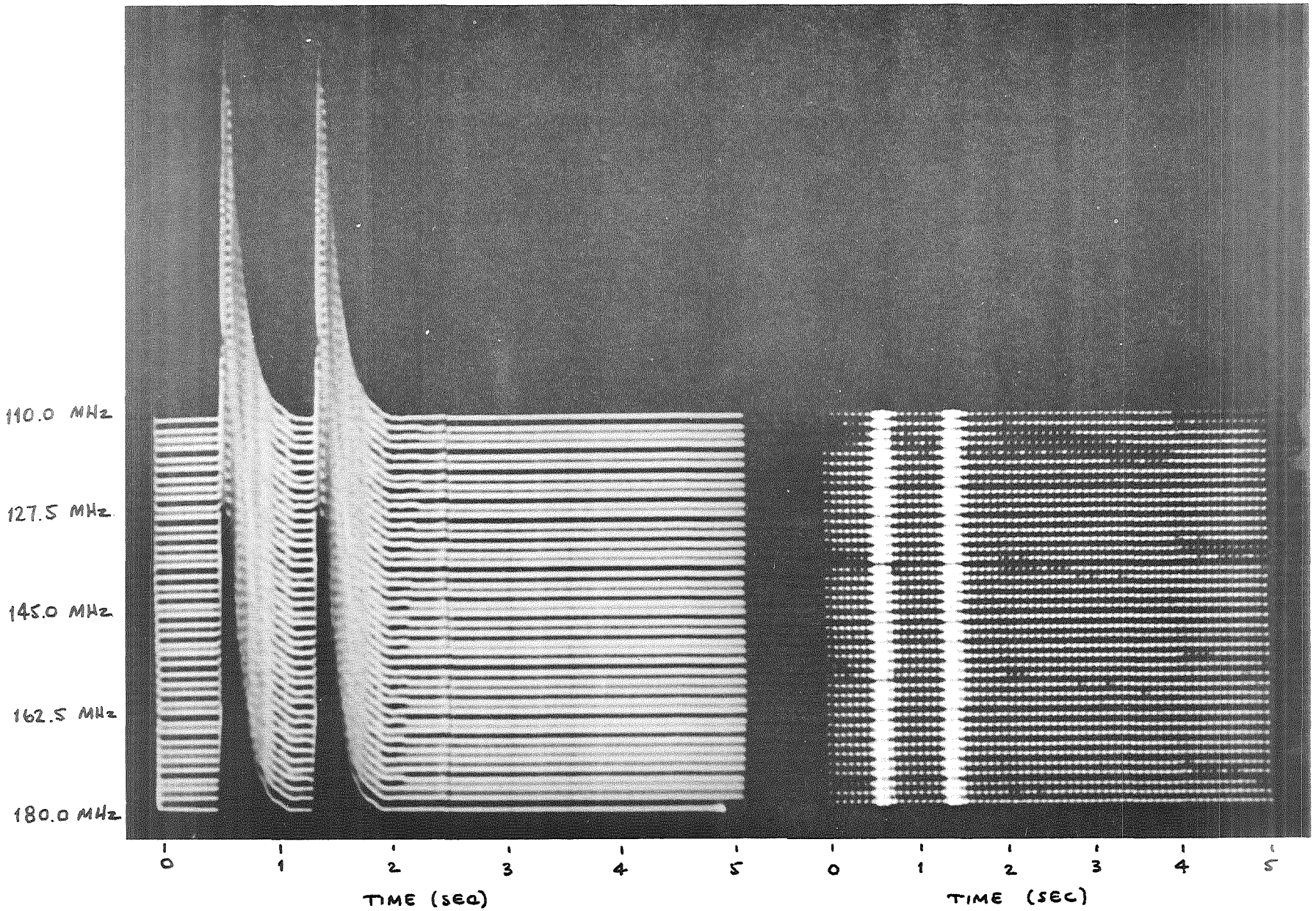

Fig. 25. - Same as Fig. 24, but with two separate Type III bursts.

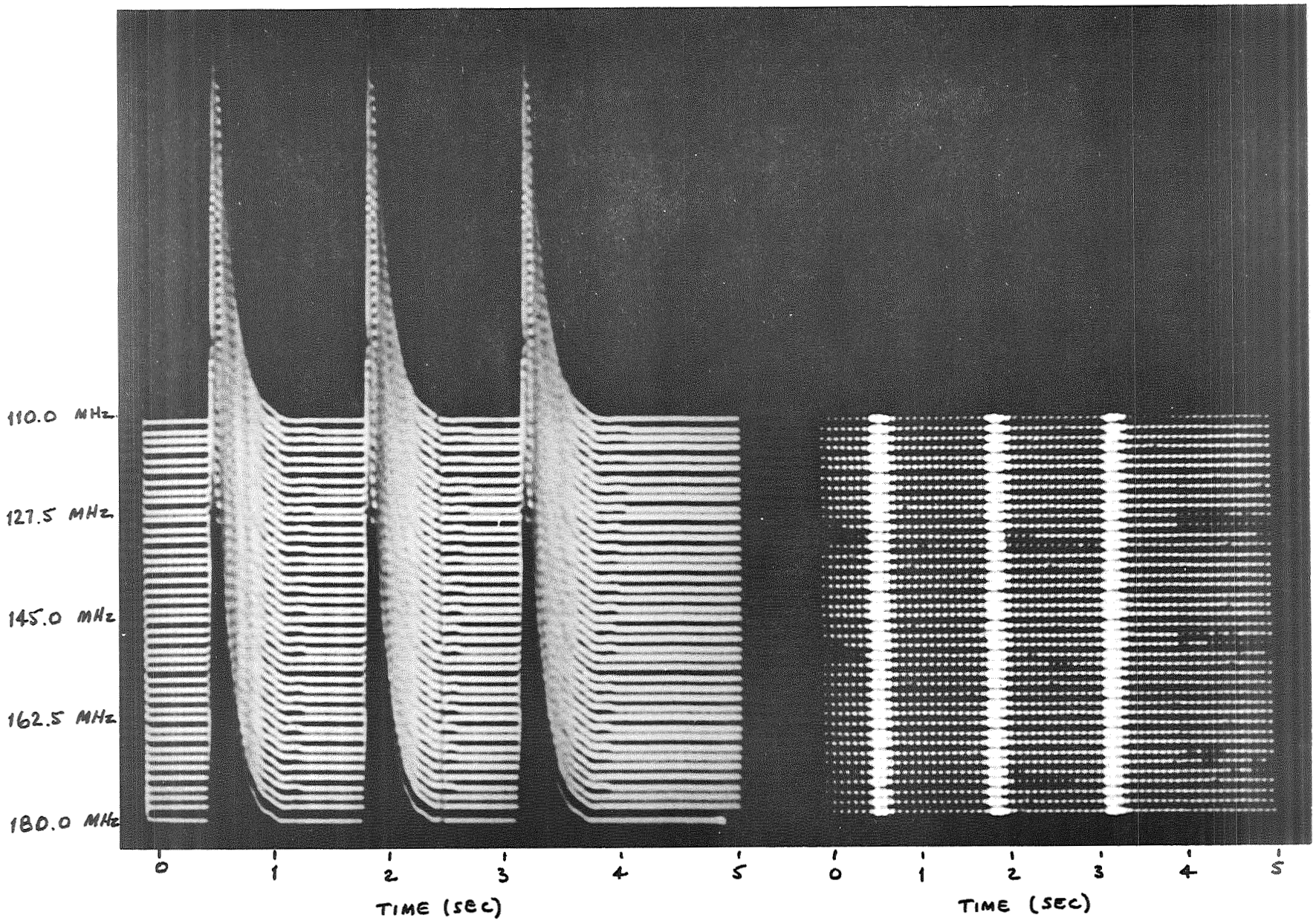

Fig. 26. - Same as Fig. 24, but with three separate Type III bursts.

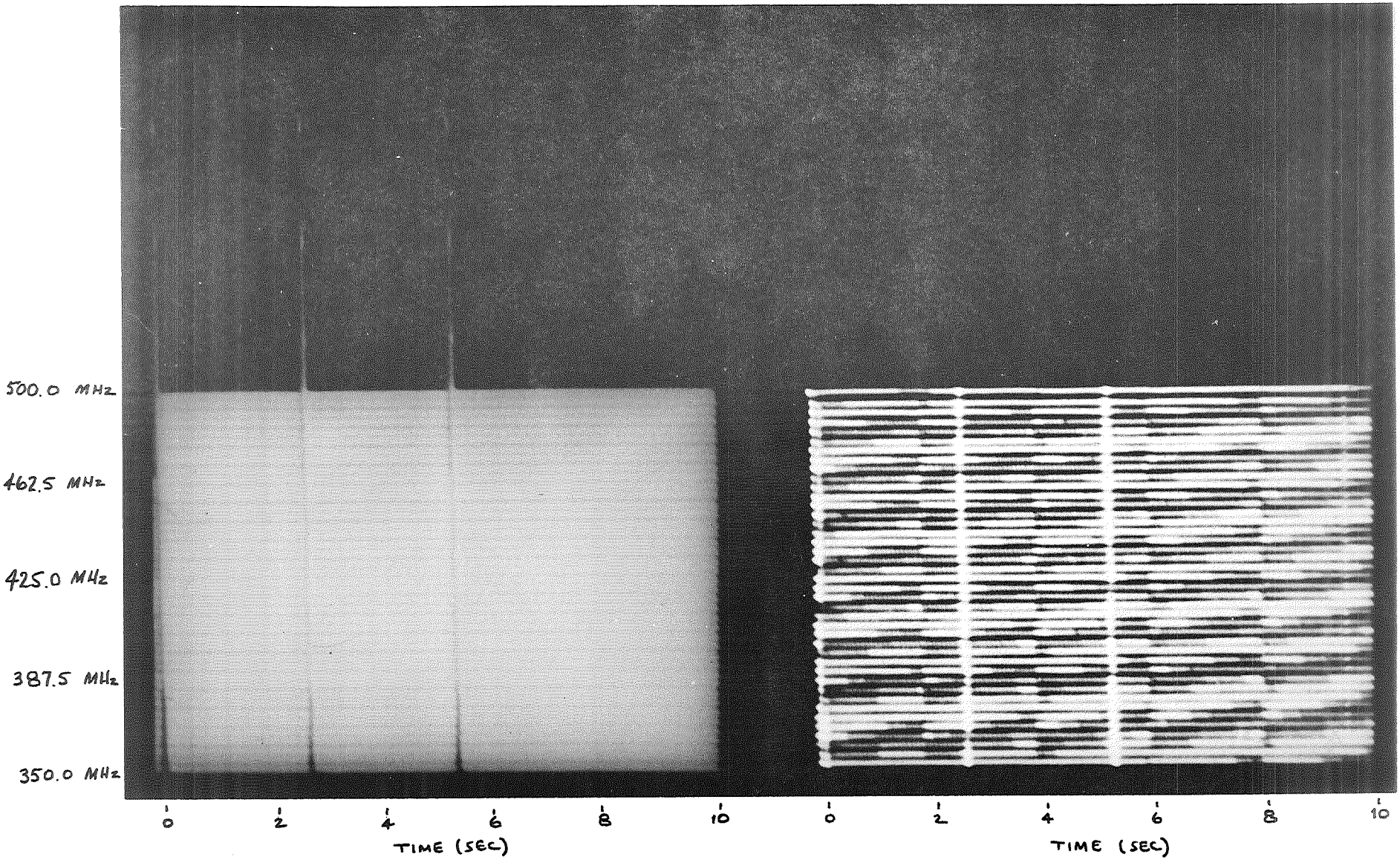

Fig. 27. - Computed dynamic spectrum over the frequency band 500 - 350 MHz - first example.

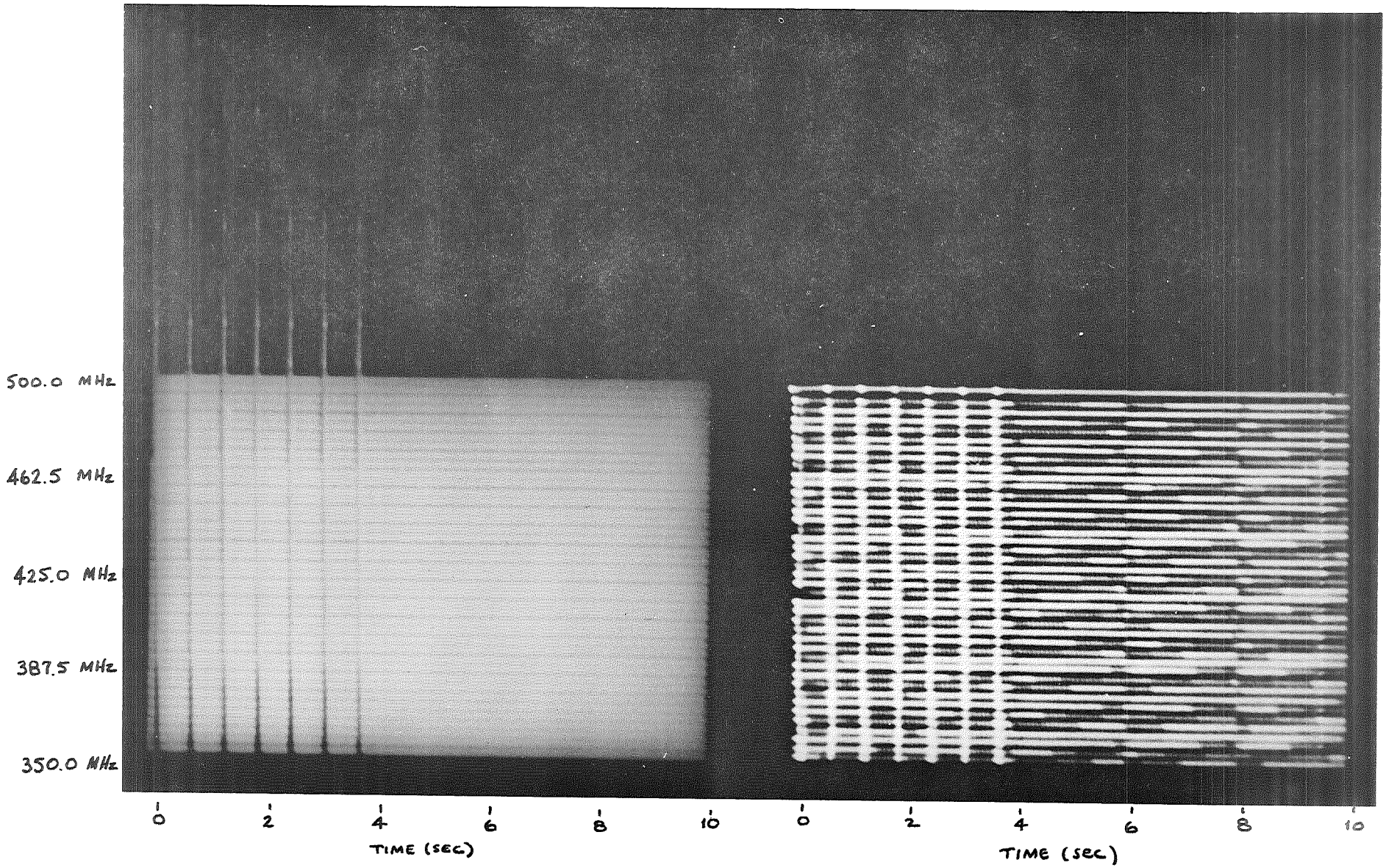

Fig. 28. - Computed dynamic spectrum over the frequency band 500 - 350 MHz - second example.

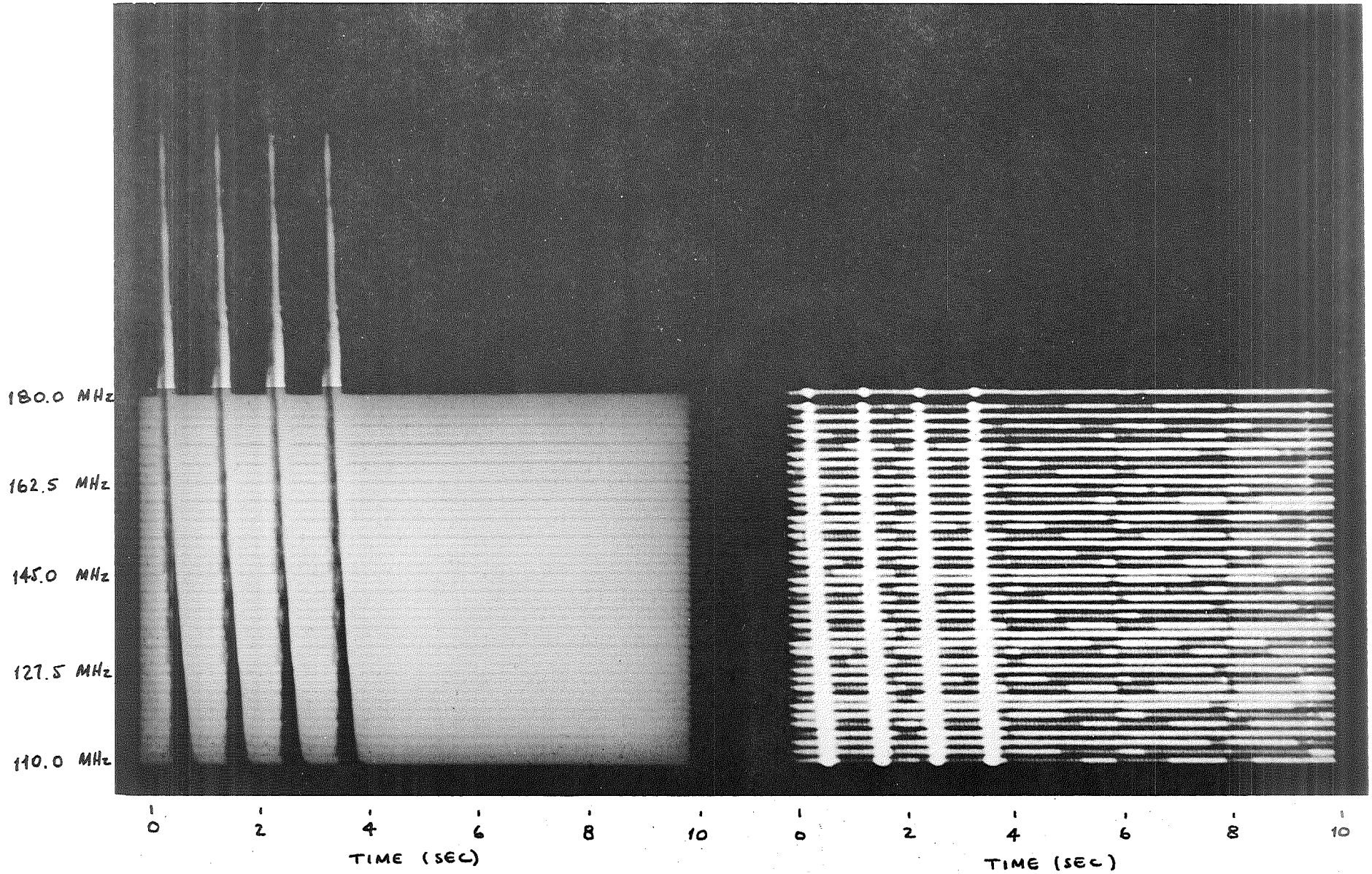

Fig. 29. - Computed dynamic spectrum over the frequency band 180 - 110 MHz - fifth example.

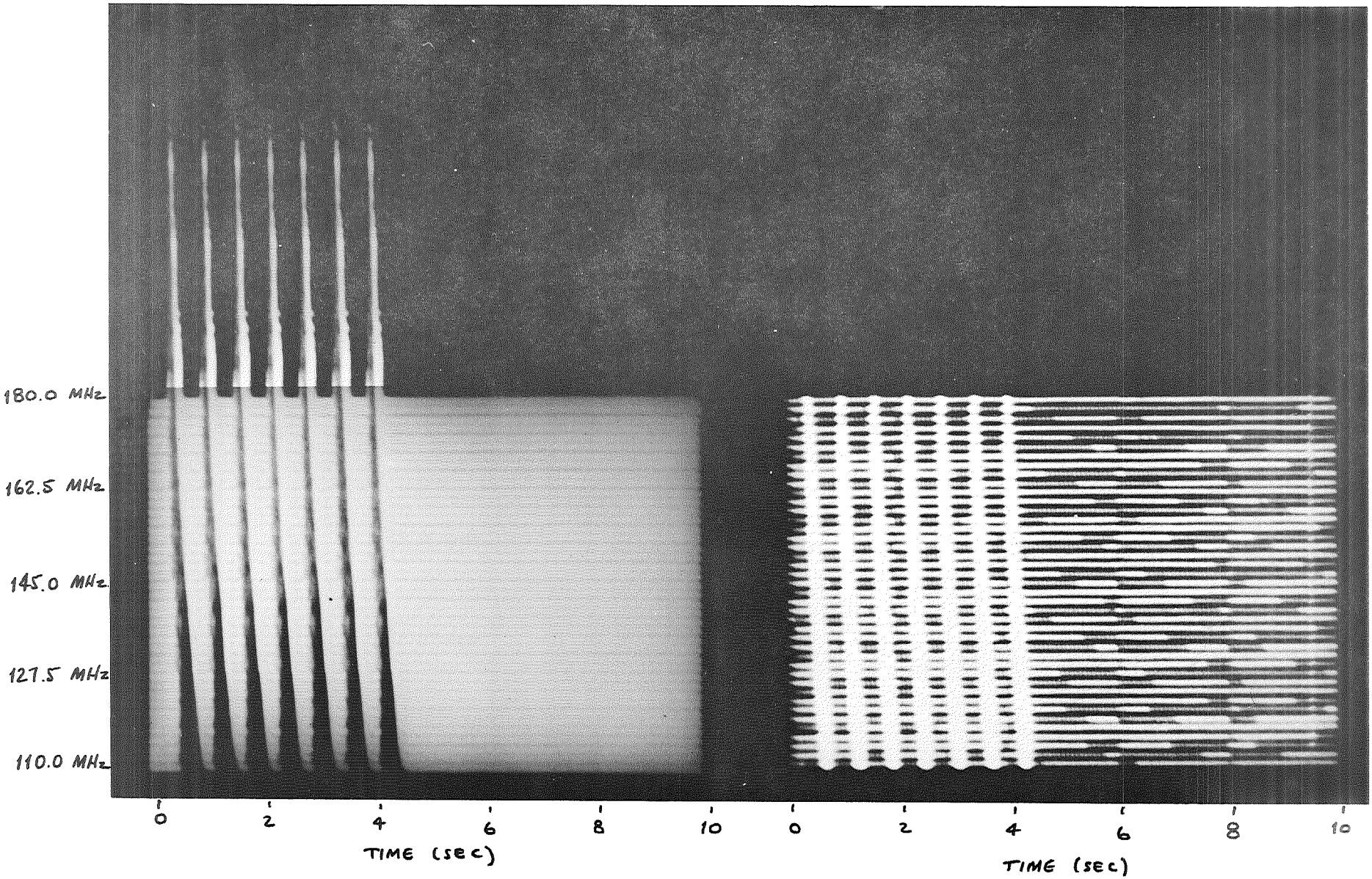

Fig. 30. - Computed dynamic spectrum over the frequency band 180 - 110 MHz - sixth example.

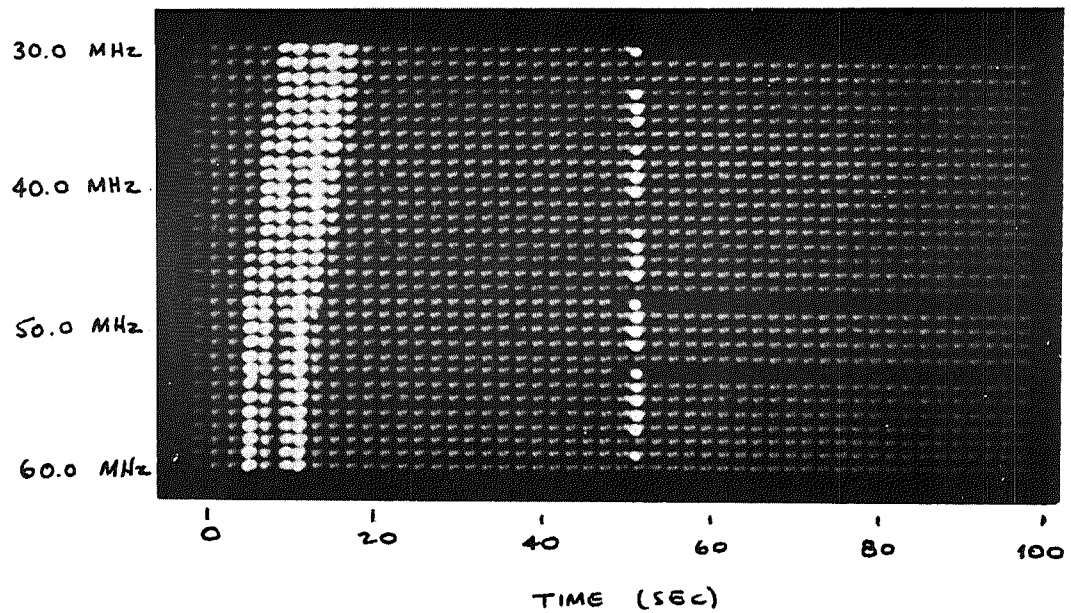

Fig. 31. - Computed dynamic spectrum over the frequency band 60 - 30 MHz.

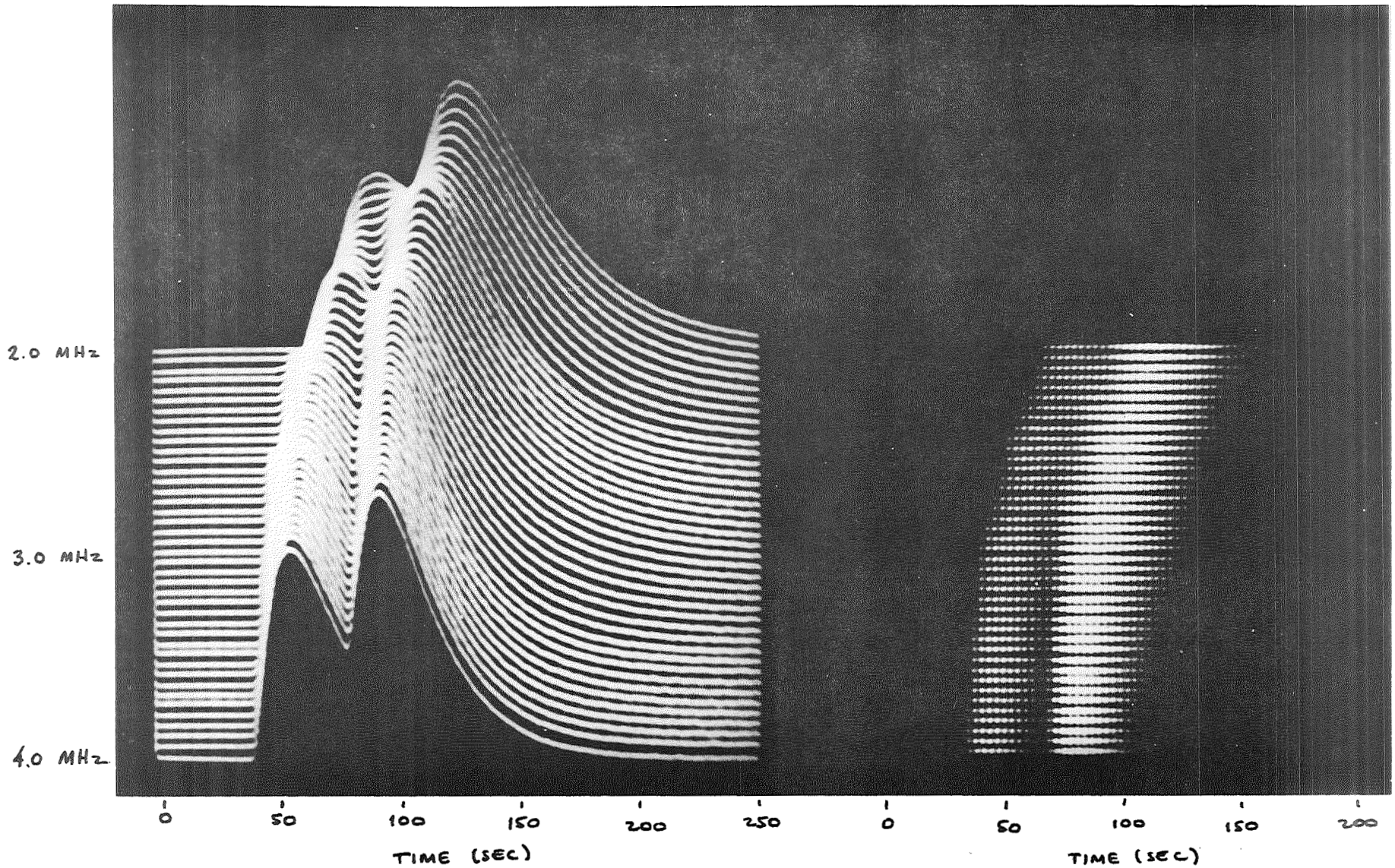

Fig. 32. - Computed dynamic spectrum of double Type III burst over the frequency band 4-2 MHz.

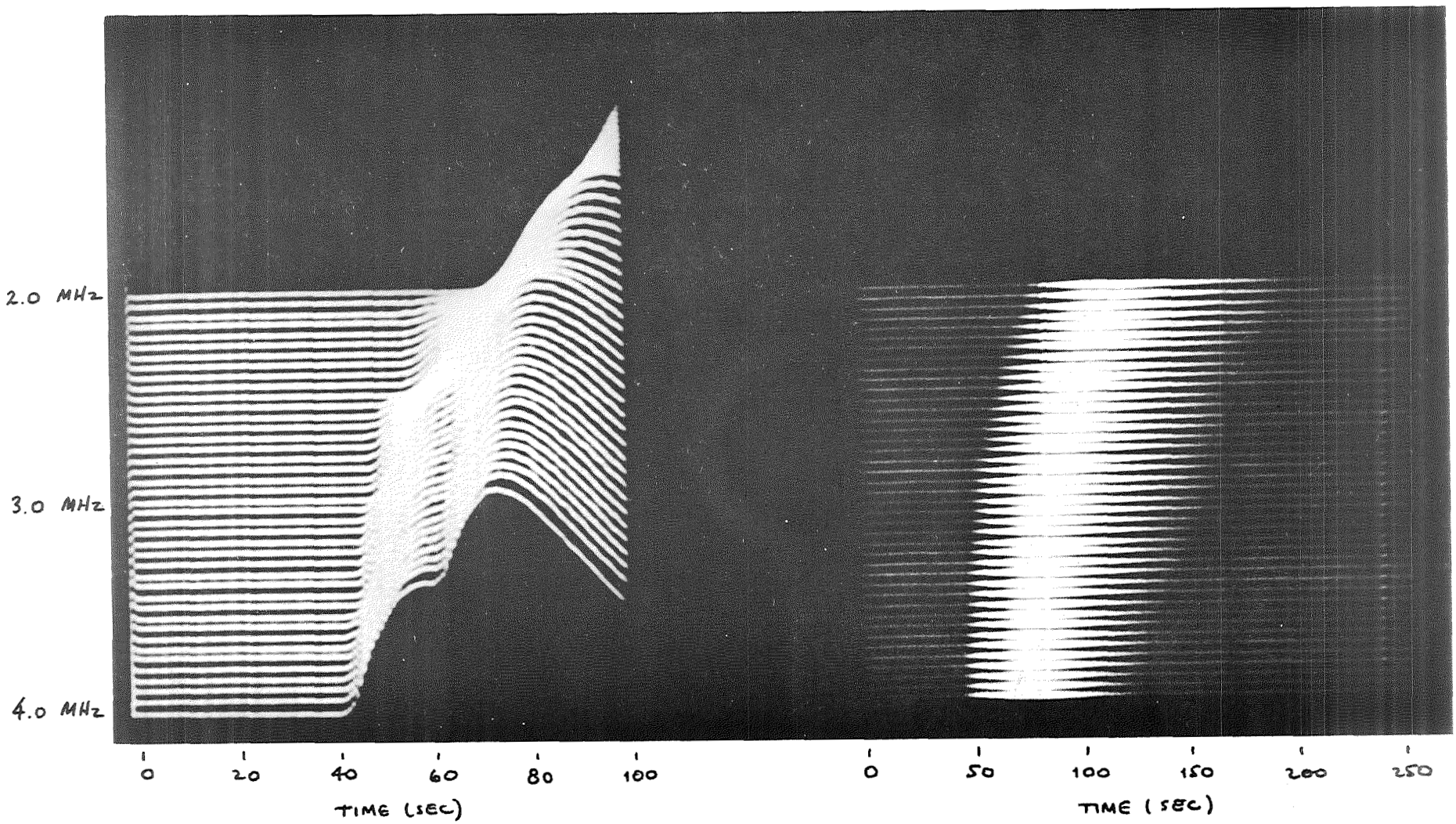

Fig. 33. - Computed dynamic spectrum of merged double Type III burst over the frequency band 4-2 MHz.

IV. CONCLUSION

The results presented here indicate that the computation of solar burst time profiles and dynamic spectra, utilizing a model of the form described, can produce theoretical values for Type III burst characteristics which agree quite well with observational values. The parameters which have been used in the model can then be regarded as indicative of coronal physical conditions and of Type III solar burst radiation mechanisms. Specifically, the computations suggest that

(i) The average density structure of the enhanced corona from which radio bursts originate is that illustrated in Figure 1.

(ii) One or more additional wave damping mechanisms is required if the discrepancy between temperatures measured in the far corona and those implied from radio burst durations is to be resolved.

(iii) The suprathermal electron velocity spectrum has a velocity width of approximately 0.15 c and a maximum injection velocity of approximately 0.37 c. The maximum velocity decreases with increasing radial distance from the point of injection.

(iv) The amplitude transfer function as defined herein has a value which is shown by computation to be much nearer 9 than to 4 or 1.

(v) The intrinsic frequency bandwidth of Type III bursts is within the range (0.05 - 0.20)fp, and has a best-fit value of 0.15 fp.

Perhaps the most interesting result of this work is that a high level of accuracy was obtained in matching observations, even though the model which was used did not treat the difficult plasma physics problems in a realistic way. As some of the present variables in the problem become known, the remainder should be increasingly easy to determine. In this connection, the following points are relevant.

(i) A low-frequency (<5MHz) interferometric observation of a Type III burst would do a great deal toward determining the density gradient in the intermediate and far corona. Any such observation would be of great interest, but would require two spacecraft with substantially different position angles.

(ii) Figure 9 suggests a form for the diffusion of high-velocity electrons in the corona. If such a result can be combined with velocity spectrum measurements at 1A.U., it may be possible to determine a satisfactory interplanetary diffusion model.

(iii) Observations with high spatial resolution (<6' at 40 MHz, if possible) should be made in an attempt to determine the intrinsic bandwidths of Type III bursts. Such information would be of substantial aid in the development of the plasma physics needed to describe the solar radiation.

In conclusion it should be noted that the results presented here refer to "average" Type III bursts. Any individual event is likely to result from an electron velocity spectrum which differs from the average, may occur with a density enhancement differing from the model described here, etc. Observers familiar with actual spectral records are aware also that few real events are as clean and precise as those illustrated here. The total problem is complex; it is hoped that this work will prove to be a worthwhile step toward its solution.

LIST OF REFERENCES

Billings, D. E. 1966, A Guide to the Solar Corona (New York: Academic Press).

Boischot, A. 1967, Ann.d'Ap., 30, 85.

_____, Lee, R. H., and Warwick, J. W. 1960, Ap.J., 131, 61.

Elgaroy, O 1965, Solar System Radio Astronomy, ed. J. Aarons, (New York: Plenum Press), 201.

_____, and Rodberg, H. 1963, Astrophys. Norvegica, 8, 271.

Graedel, T.E. 1969, Unpublished Ph.D. Dissertation, University of Michigan

Haddock, F. T., and Graedel, T. E. 1968, Paper presented at the 127th Meeting of the American Astronomical Society, Victoria, B.C., August 21, 1968.

Hartz, T. R. 1964, Ann.d'Ap., 27, 831.

_____. 1966 Privately circulated manuscript cited in Newkirk, G. A., Jr., Ann Rev. Astr. and Ap., Vol V, ed. L. Goldberg (Palo Alto, Calif.:Annual Reviews, Inc.), 214.

_____. 1969, Planet Sp. Sci., 17, 267.

Hughes, M. P., and Harkness, R. L. 1963, Ap. J., 138, 239.

Jaeger, J. C., and Westfold, K. C. 1949, Austr. J. Sci. Res., A2, 322.

Malitson, H. H., and Erickson, W. C. 1966, Ap. J., 144, 337.

Malville, J. M. 1962, Ap. J. 136, 266.

_____, 1967, Solar Phys., 2 , 484.

Ness, N. F., Scearce, C. S., and Seek, J. B. 1963, J. Geophys. Res., 69, 3531.

Neugebauer, M., and Snyder, C. W. 1966, The Solar Wind, ed. R. J. Macklin, Jr. and M. Neugebauer (Pasadena, Calif: Jet Propulsion Laboratory and California Institute of Technology), 3.

Newkirk, G. A., Jr. 1961, Ap. J. 133, 983.

_____. 1967, Ann. Rev. Astr. and Ap. Vol. V, ed. L. Goldberg (Palo Alto, Calif.: Annual Reviews, Inc.), 214.

Payne-Scott, R., Yabsley, D. E., and Bolton, J. G. 1947, Nature, 160, 256.

Pneuman, G. W. 1968, Solar Physics, 3, 578.

_____. 1969, Solar Physics, 6, 255.

Pottasch, S. R. 1960, Ap. J., 131, 68.

Scarf, F. L., and Noble, L. M. 1965, Ap. J., 141, 1479.

Slysh, V. I. 1967a, Cosmic Res., 5, 759.

_____. 1967b, Sov. Astr.-A.J., 11, 389.

Stone, R. G. 1969, Paper presented at the Spring Meeting of U.R.S.I., Washington, D. C., April 21, 1969.

Sturrock, P. A., and Smith, S. M. 1968, Solar Phys., 5, 87.

Tousey, R. 1969, Private Communication.

Weiss, A. A., and Sheridan, K. V. 1962, J. Phys. Soc. Japan, 17, A-II, 223.

_____, and Wild, J. P. 1964, Austr. J. Phys., 17, 282.

Whang, V.C., Liu, C. K., and Chang, C. C. 1966, Ap. J., 145, 255.

Wild, J. P. 1950, Austr. J. Sci. Res., A3, 541.

_____, Sheridan, K. V., and Neylan, A. A. 1959, Austr. J. Phys., 12, 369.

_____, Smerd, S. F., and Weiss, A. A. 1963, Ann. Rev. Astr. and Ap., Vol.I, ed. L. Goldberg (Palo Alto, Calif.: Annual Reviews, Inc.), 291.

Williams, S. E. 1948, Nature, 162, 108.

Zaitsev, V. V., and Kaplan, S. A. 1966, Astrofizika, 2, 169.